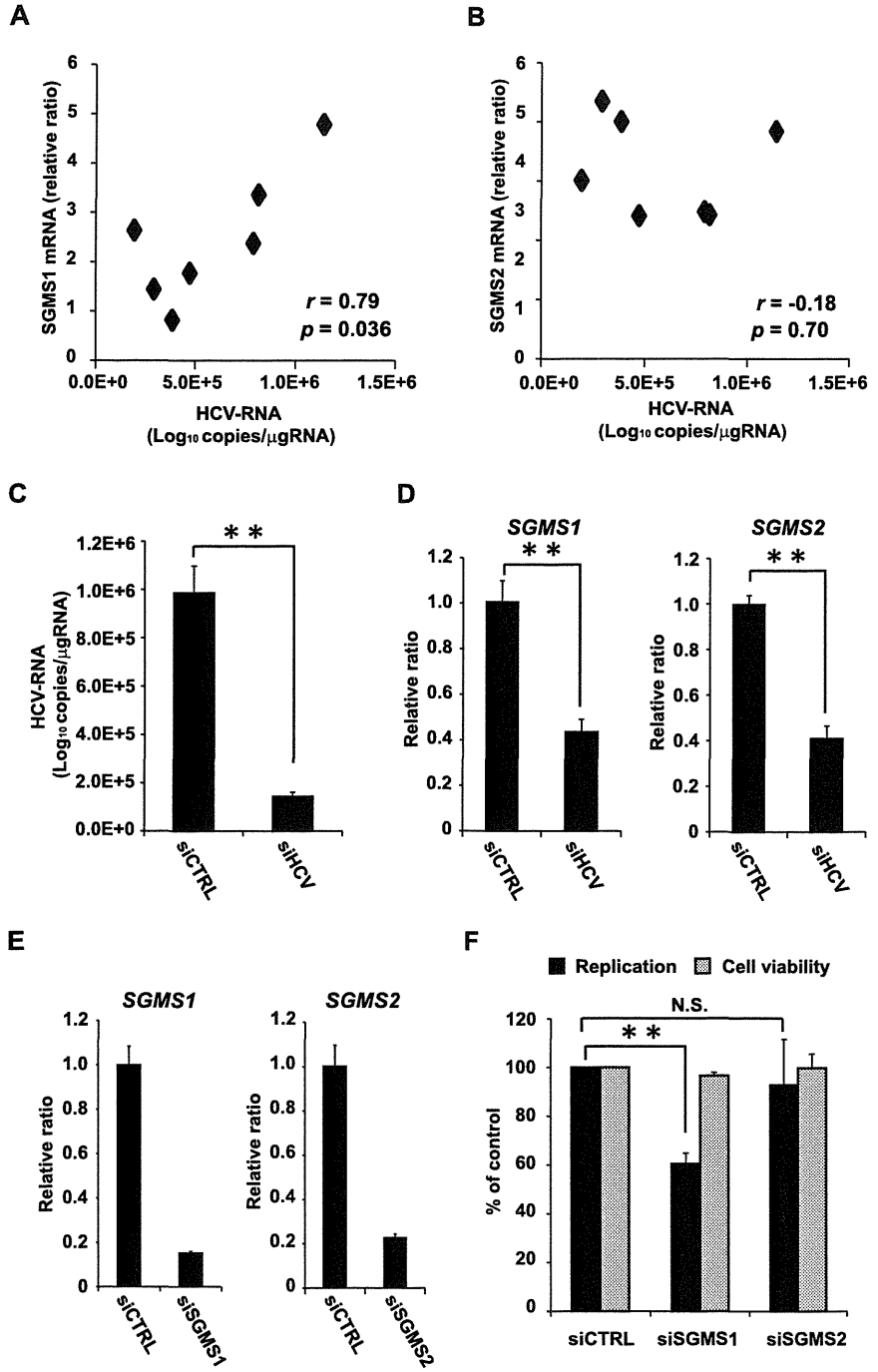

Figure 2. Relationship between the SGMS genes and HCV infection. (**A, B**) The correlation between SGMS1/2 and liver HCV-RNA of HCV infected humanized chimeric mice (n = 7). (**C**) The effect of silencing HCV genome RNA with siRNA (siE-R7: 1 nM) on HCV in HCV-infected cells. (**D**) The effect of silencing HCV genome RNA with siRNA (siE-R7: 1 nM) on the expression of SGMS1/2 mRNA measured by RTD-PCR. (**E**) The effect of silencing SGMS1/2 mRNA with siRNA (3 nM each) measured by RTD-PCR. (**F**) The effect of silencing SGMS1/2 mRNA with siRNA (3 nM) on HCV replication in FLR 3-1. In all cases, error bars indicate SDs. *$p<0.05$ and **$p<0.01$.
doi:10.1371/journal.ppat.1002860.g002

Inhibition of sphingolipid biosynthesis impedes HCV infection of chimeric mice

To evaluate the effects of inhibition of sphingolipid biosynthesis in an animal model, we administered NA808 or pegylated interferon-α (PegIFN-α) via intravenous or subcutaneous injection to HCV-infected chimeric mice harboring human hepatocytes (**Table S2**). In chimeric mice infected with HCV genotype 1a, NA808 treatment led to a rapid decline in serum HCV-RNA (approximately 2–3 log units within 14 days). On the other hand, PegIFN-α produced less than a 1 log unit reduction, despite being delivered at 20 times the typical clinical dose (**Figure 4A**). Furthermore, results of 21-day NA808 treatment (5 mg/kg) in individual mice indicated that serum HCV RNA continued to decrease in all chimeric mice without viral breakthrough

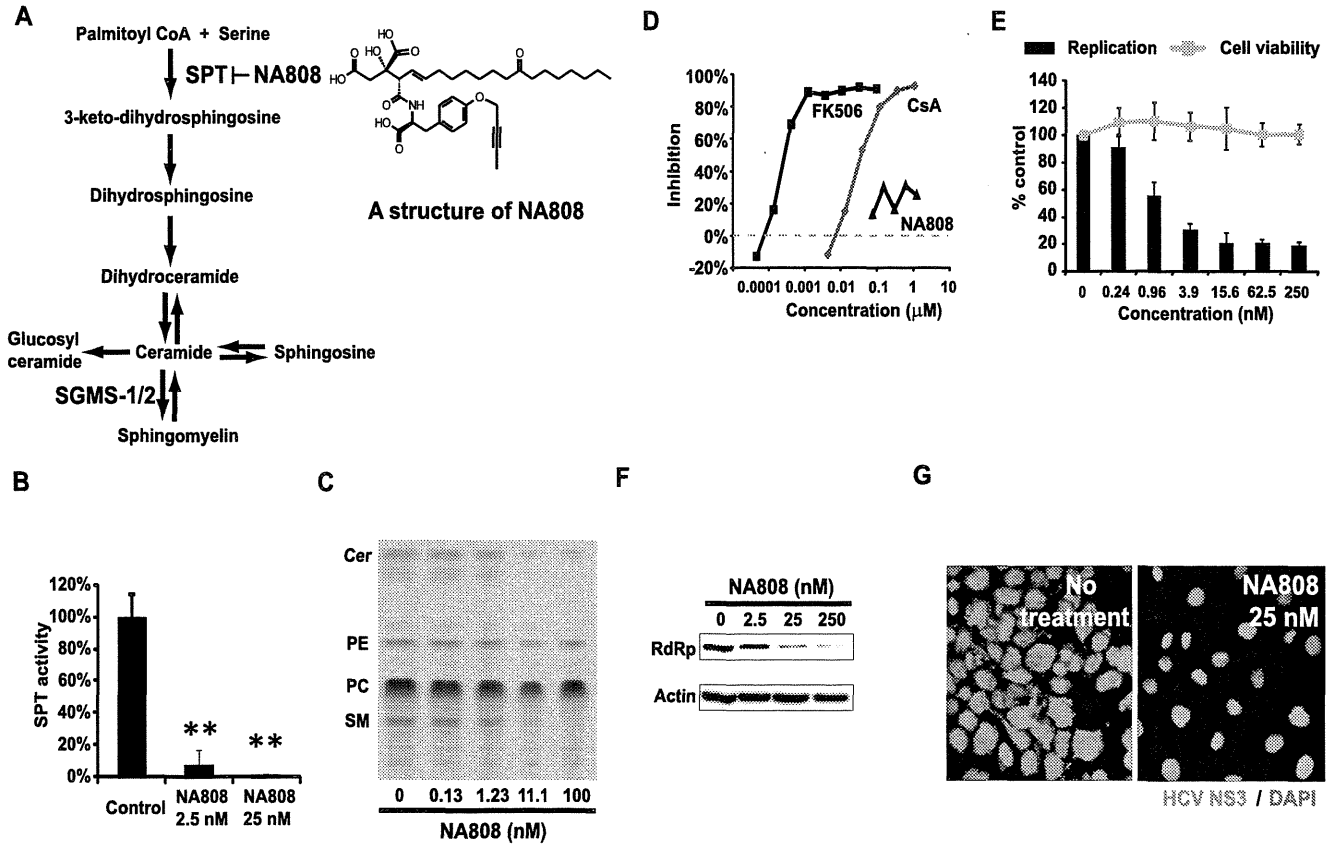

Figure 3. Characterization of the hepatotropic serine palmitoyltransferase inhibitor NA808. (**A**) Sphingolipid biosynthesis pathway and structure of NA808. (**B**) Activity of SPT in FLR3-1 cells after 72 h of NA808 treatment. $^{**}p<0.01$ compared with control. (**C**) Results of TLC showing *de novo* sphingolipid biosynthesis in the presence of NA808. Cer = ceramide, PE = phosphatidylethanolamine, PC = phosphatidylcholine, SM = sphingomyelin. (**D**) Immunosuppressive activity of NA808. Cyclosporin A (CsA) and tacrolimus (FK-506) were used as positive controls. (**E**) Effects of NA808 on HCV replication (black bars) and cell viability (gray symbols) in FLR 3-1 replicon-containing cells. Error bars indicate SDs. (**F**) Effects of NA808 on the level of the RdRp and β-actin, as assessed by Western blotting. (**G**) Effect of NA808 on the production of HCV NS3 protein (green) in FLR3-1 replicon-containing cells, as assessed by immunofluorescence analysis. Nuclear DNA was stained with DAPI (blue).
doi:10.1371/journal.ppat.1002860.g003

(**Figure 4B**). Notably, in 2 of 5 chimeric mice, serum HCV-RNA was not detectable at the end of the 21-day regimen. Consistent with this observation, the levels of both hepatic HCV-RNA and HCV core protein decreased significantly ($p<0.01$ and $p<0.05$, respectively) following NA808 treatment, these effects being dose dependent (**Figure 4C**). Immunofluorescence analysis and immunohistochemistry confirmed the reduced abundance of HCV core protein after 14 days of treatment (**Figure 4D and Figure S3**).

In genotype 2a-infected chimeric mice, NA808 decreased serum HCV-RNA by approximately 3 log units within 14 days (**Figure 4E**). NA808-treated mice displayed a corresponding reduction in hepatic HCV-RNA (**Figure 4F**). NA808 did not affect body weight or human serum albumin levels (**Figures S4A and S4B**). Furthermore, hematoxylin and eosin (H&E) staining revealed little morphological change in response to treatment with NA808. Immunofluorescence analysis also indicated that NA808 did not affect the production of human albumin (**Figure S4C**). Thus, inhibition of sphingolipid biosynthesis by an SPT inhibitor impeded HCV replication in an animal infection model, regardless of HCV genotype.

Inhibition of SPT decreases ceramide and SM levels in hepatocytes of humanized chimeric mice

We next investigated the effects of sphingolipid biosynthesis inhibition on SM and ceramide levels in hepatocytes of humanized chimeric mice. Pharmacokinetic analysis in a rat model indicated that NA808 has hepatotropic properties (**Table S1**). Consistent with this analysis, our study in chimeric mice also indicated that the NA808 concentration was much higher in the liver than in serum (**Figure S5**). Furthermore, we observed that serum SM content was not decreased by NA808 treatment (**Figure S6**), in contrast to the effects previously observed for myriocin, another SPT inhibitor [19].

In HCV-infected chimeric mouse hepatocytes, MS analysis indicated that HCV infection resulted in increased ceramide and SM levels. However, treatment of infected animals with NA808 (5 mg/kg) attenuated this increase in ceramide and SM levels in hepatocytes, and the change in SM was significant ($p<0.05$) compared to the level observed in HCV-infected chimeric mice with no treatment. This effect of NA808 on ceramide and SM levels was dose-dependent (**Figures 5A and 5B**). We also found that SM levels and hepatic HCV-RNA were correlated (**Figure 5C**).

Interestingly, treatment with NA808 effectively decreased two specific SM and ceramide molecular species (*d*18:1-22:0 and *d*18:1-24:0), slightly decreased one other species (*d*18:1-24:1), and hardly decreased another (*d*18:1-16:0). Further, we found that among SM and ceramide molecular species, *d*18:1-16:0 did not change (**Figures 5D and 5E**). These results indicate that the

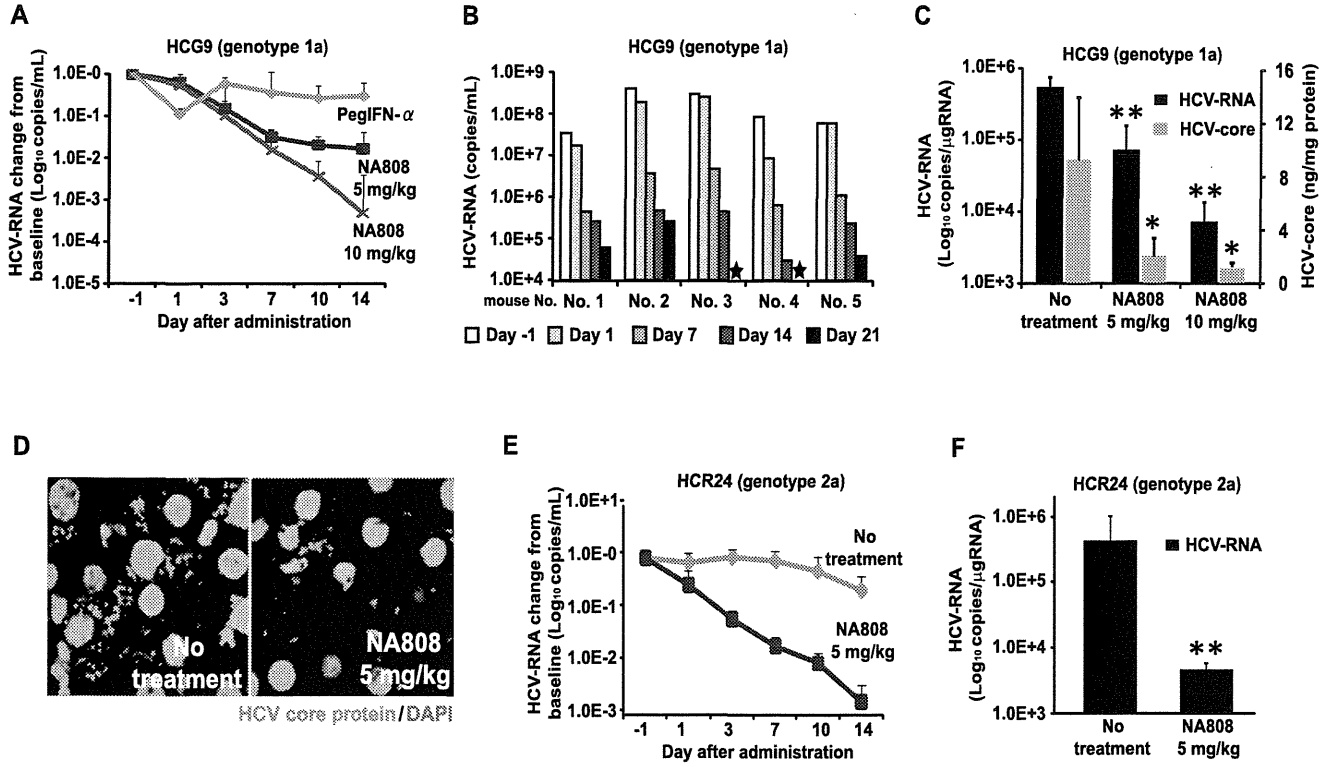

Figure 4. Inhibition of sphingolipid biosynthesis with hepatotropic serine palmitoyltransferase (SPT) inhibitor NA808 exerts anti-HCV effect. (**A**) Serum HCV-RNA levels in response to treatment with NA808 (blue, 5 mg/kg/day, purple, 10 mg/kg/day, n = 6 each), or PegIFN-α (pink, 30 μg/kg twice weekly, n = 4). (**B**) Effect of NA808 (5 mg/kg/day) on serum HCV-RNA levels. A star indicates that HCV-RNA was not detected. (**C**) Levels of liver HCV-RNA (black) and HCV core protein (gray) after the 14-day treatment. *$p<0.05$ and **$p<0.01$ compared with no treatment. (**D**) Histological analysis using immunofluorescent labeling of HCV core protein (green) and fluorescent staining of nuclei (blue). (**E**) Serum HCV-RNA levels in response to no treatment (pink, n = 3) or NA808 treatment (blue, 5 mg/kg/day, n = 4). (**F**) Liver HCV-RNA levels in genotype 2a-infected mice after the 14-day treatment. *$p<0.05$ and **$p<0.01$ compared with no treatment. In all cases, error bars indicate SDs.
doi:10.1371/journal.ppat.1002860.g004

effects of sphingolipid biosynthesis inhibition varied among the molecular species.

Considering these results, we found a discrepancy in SM molecular species which were considered to be important for HCV replication. To elucidate the relationship between SM molecular species and HCV replication, we attempted to identify endogenous SM molecular species comprising the DRM fraction and to evaluate the effects of HCV infection and inhibition of sphingolipid biosynthesis on SM levels of the DRM.

Relationship between endogenous SM molecular species constituting the DRM and HCV replication

We previously reported that SM interacts with RdRp, allowing it to localize to the DRM fraction where HCV replicates and activates RdRp [7,8], and that suppression of SM biosynthesis disrupts the association between RdRp and SM in the DRM fraction, resulting in suppression of HCV replication [7,8]. In the present study, treatment with NA808 decreased SM levels in the DRM fraction; the decreased presence of SM correlated with decreased RdRp abundance, but the same effect was not seen for HCV nonstructural protein 3 (**Figures S7A–C**). Given these results, we investigated whether HCV replication was induced by elevated SM levels. Specifically, we compared SM levels in the DRM fraction between HCV-infected hepatocytes and uninfected hepatocytes. MS analysis showed that HCV increased SM levels in the DRM fraction more remarkably than in whole cells (**Figure 6A**). Next, we identified SM molecular species composing the DRM fraction and found that the composition ratio of SM molecular species was distinct between whole cells and DRM fractions in both HCV-infected and uninfected hepatocytes (**Figure 6B and Figure S8**). The DRM was composed primarily (69%) of *d*18:1-16:0, followed (in decreasing order) by *d*18:1-24:0, *d*18:1-22:0, and *d*18:1-24:1; the abundance of all SM molecular species increased upon HCV infection (**Figure 6C**). Further, NA808 treatment decreased all SM molecular species in the DRM fraction. Consistently, NS3 protease inhibitor decreased all SM molecular species in the DRM fraction of subgenomic replicon cells (**Figure S9**).

To address the association between RdRp and the endogenous SM molecular species composing the DRM, we used high-performance liquid chromatography (HPLC) to separate each SM molecular species from bulk SM derived from bovine milk and brain. We evaluated the relationship between RdRp and these endogenous SM molecular species using *in vitro* analysis. Enzyme-linked immunosorbent assay (ELISA) indicated that these endogenous SM molecular species bound to RdRp more readily than the bulk SM derived from milk as a positive control (**Figure 6D**). Further, *in vitro* HCV transcription analysis showed that three SM species (*d*18:1-16:0, *d*18:1-22:0, and *d*18:1-24:1) increased *in vitro* RdRp activation by approximately 5-fold, whereas the *d*18:1-24:0 species increased activation by 2-fold (**Figure 6E**). In a previous study, the soluble RdRp without its C-terminal hydrophobic 21-amino-acid sequence was used in *in vitro* analysis [8], and whether the relationship between RdRp and SM proved in this analysis

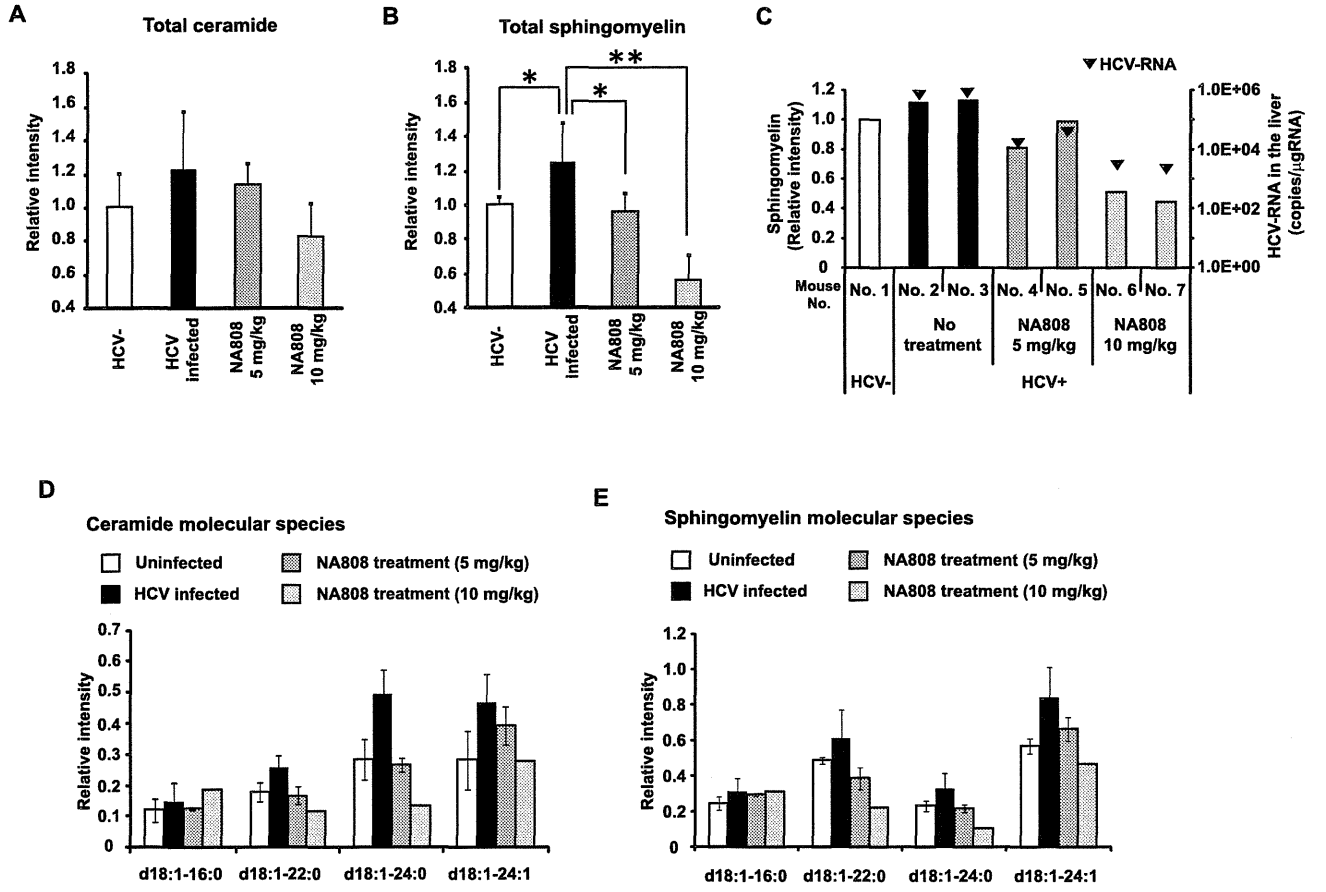

Figure 5. Effects of NA808 treatment on sphingomyelin (SM) and ceramide (total and individual molecular species). (**A, B**) Relative ratio of total ceramide (**A**) and SM (**B**) in uninfected mice (white, n = 4), HCV genotype 1a-infected mice (black, n = 5), and HCV-infected mice treated with NA808 for 14 days (dark gray, 5 mg/kg, n = 4; light gray, 10 mg/kg, n = 3). *$p<0.05$ and **$p<0.01$ compared with HCV-infected mice. (**C**) SM levels (bars) and HCV RNA levels (black arrowhead) in the livers of mice treated for 14 days with NA808 (5 or 10 mg/kg/day) and untreated chimeric mice. (**D, E**) Relative intensities of individual ceramide molecular species (**D**) and individual SM molecular species (**E**) in uninfected mice (white, n = 3), HCV-infected mice (black, n = 3), and HCV-infected mice treated with NA808 for 14 days (dark gray, 5 mg/kg, n = 2; light gray, 10 mg/kg, n = 1). In all cases, error bars indicate SDs.
doi:10.1371/journal.ppat.1002860.g005

reflected the state in the membranous replication complex remains to be elucidated. Therefore, we attempted to examine the effect of endogenous SM molecular species on HCV replicase activity *in vivo* using digitonin-permeabilized semi-intact replicon cells, which permit monitoring of the function of the active HCV replication complex (**Figure 6F**) [20]. This *in vivo* analysis also enabled us to deliver the extrinsically added SM molecular species directly to the cytosol. This RNA replication assay indicated that the endogenous SM molecular species (*d*18:1-16:0 and *d*18:1-24:0) enhanced HCV-RNA replication, these species being consistent with the two SM molecular species that primarily constitute the DRM and are decreased significantly by NA808 treatment (**Figures 6G and 6H**). These results suggest that HCV infection modifies the levels of specific endogenous SM molecular species, which in turn enhance HCV-RNA replication by interacting with RdRp.

Discussion

In this study, we showed that HCV alters sphingolipid metabolism, resulting in a better environment for viral replication. Specifically, HCV increased SM content in the DRM fraction; this step is essential for viral replication since SM is a key component of the membranous replication complex and interacts with RdRp. Employing MS analysis, we identified endogenous SM molecular species (located in the DRM fraction) that increased upon HCV infection, and demonstrated that these endogenous SM molecular species interact directly with RdRp, enhancing HCV replication. Thus, we concluded that HCV modulates sphingolipid metabolism to promote viral replication.

We found that the expression levels of SGMS1/2 and the content of SM and ceramide in HCV-infected humanized chimeric mouse livers was increased (Figure 1). Our measurement revealed that chronic HCV infection promoted sphingolipid biosynthesis. HCV is known to induce cellular stress [21,22]. A variety of cell stressors increase intracellular ceramide content during the execution phase of apoptosis [23,24], indicating that ceramide is a proapoptotic lipid mediator. Furthermore, activation of ceramide-metabolizing enzymes such as glucosylceramide synthase and SM synthase can attenuate apoptosis by decreasing the intracellular ceramide content [25,26]. We found that HCV infection correlated with increased mRNA levels of the genes that encode human SM synthases (*SGMS1/2*) and glucosylceramide synthase (*UGCG*) (data not shown). Thus, the increase in ceramide levels observed in our study was likely to activate enzymes that transfer ceramide to other sphingolipids. On the other hand, Diamond et al. reported on lipidomic profiling performed over the

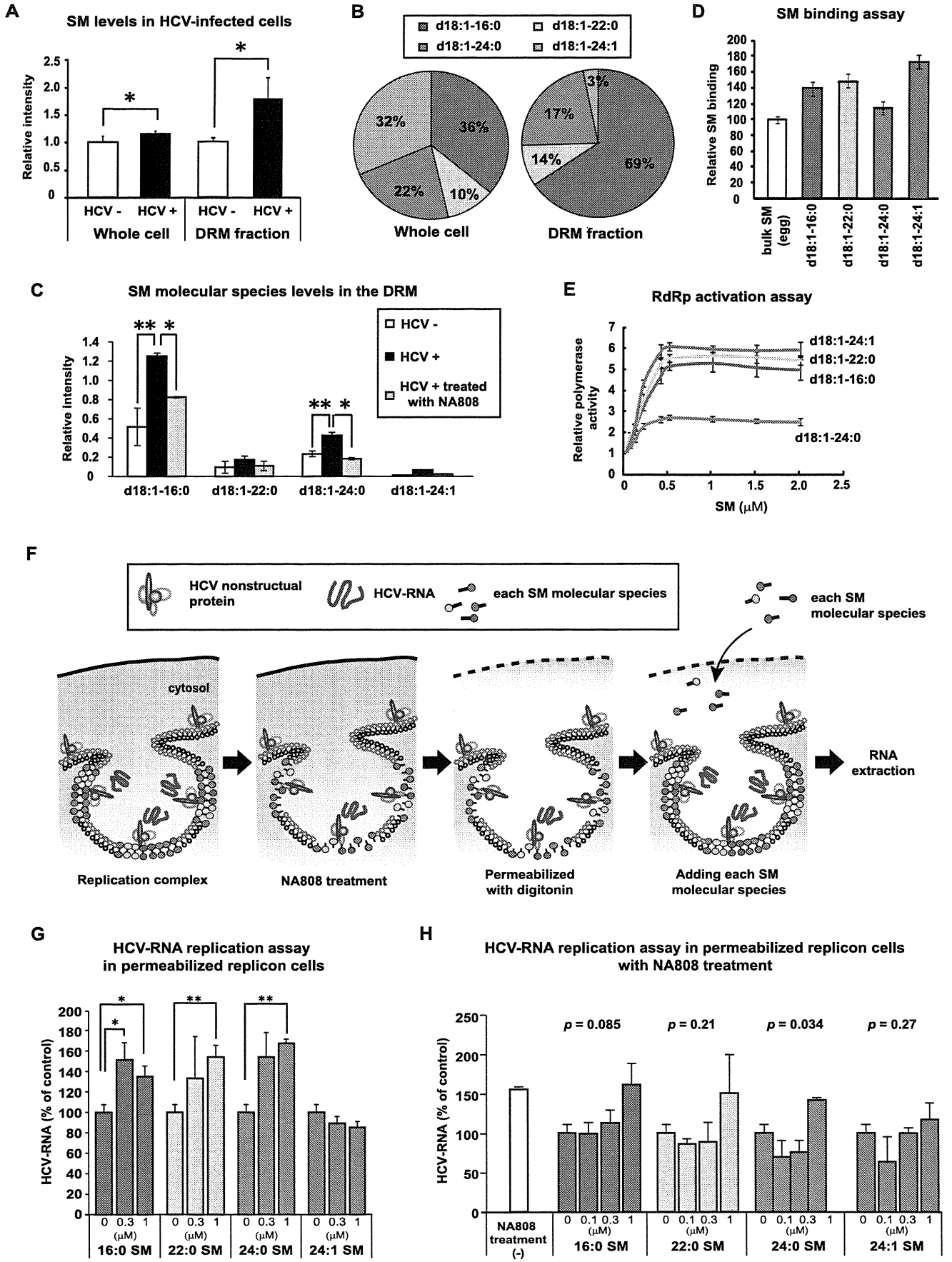
A
SM levels in HCV-infected cells
Relative intensity
HCV - HCV + HCV - HCV +
Whole cell
DRM fraction
B
d18:1-16:0
d18:1-22:0
d18:1-24:0
d18:1-24:1
32%
36%
22%
10%
3%
17%
14%
69%
Whole cell
DRM fraction
D
SM binding assay
Relative SM binding
bulk SM (egg)
d18:1-16:0
d18:1-22:0
d18:1-24:0
d18:1-24:1
C
SM molecular species levels in the DRM
Relative Intensity
HCV -
HCV +
HCV + treated with NA808
d18:1-16:0
d18:1-22:0
d18:1-24:0
d18:1-24:1
E
RdRp activation assay
Relative polymerase activity
d18:1-24:1
d18:1-22:0
d18:1-16:0
d18:1-24:0
SM (μM)
F
HCV nonstructual protein
HCV-RNA
each SM molecular species
each SM molecular species
cytosol
Replication complex
NA808 treatment
Permeabilized with digitonin
Adding each SM molecular species
RNA extraction
G
HCV-RNA replication assay in permeabilized replicon cells
HCV-RNA (% of control)
16:0 SM
22:0 SM
24:0 SM
24:1 SM
H
HCV-RNA replication assay in permeabilized replicon cells with NA808 treatment
p = 0.085
p = 0.21
p = 0.034
p = 0.27
HCV-RNA (% of control)
NA808 treatment (-)
16:0 SM
22:0 SM
24:0 SM
24:1 SM

Figure 6. Specific sphingomyelin molecular species upregulated by HCV promote HCV replication on the detergent-resistant membrane fraction. (**A**) Comparison of the relative amounts of SM, as measured by MS analysis, in whole cells and the DRM fraction of mock-infected (HuH-7 K4 cells) (white, n = 6; whole cells, n = 3; DRM fraction) and HCV (JFH-1)-infected cells (JFH/K4 cells) (black, n = 6; whole cells, n = 3; DRM fraction). (**B**) Composition ratio of SM molecular species in whole cells and DRM fraction of HCV-infected cells. (**C**) Relative intensities of each SM molecular species in the DRM fraction of mock-infected cells (white, n = 2) and HCV-producing cells without (black, n = 2) or with NA808 treatment (gray, n = 2). (**D**) Results of the ELISA SM binding assay (n = 3 each). (**E**) Average activation kinetics of each SM molecular species on HCR6 (genotype 1b) RdRp (n = 3 each). (**F**) Scheme of HCV-RNA replicase assay using digitonin-permeabilized cells. (**G, H**) Effect of each SM molecular species on HCV-RNA in digitonin-permeabilized replicon cells treated without (G) or with 10 nM NA808 (H) (n = 3 each). In all cases, error bars indicate SDs. $*p<0.05$ and $**p<0.01$.
doi:10.1371/journal.ppat.1002860.g006

time course of acute HCV infection in cultured Huh-7.5 cells and observed that specific SM molecular species were decreased 72 h after HCV infection [27]. Given that their study focused on acute HCV infection, the reason for this discrepancy may be due to the severity of infection, suggesting that the influence of HCV infection on sphingolipid metabolism differs between acute and chronic infections. We also demonstrated that HCV infection correlates with increased abundance of specific SM and ceramide molecular species, with the profiles of individual lipids differing for infection by HCG9 (genotype 1a) and HCR24 (genotype 2a). The precise mechanism and meaning of these differences remain to be elucidated.

Our results indicated that SGMS1 expression had a correlation with HCV replication. This indicates that SM synthesized by SGMS1 contributes to HCV replication. A previous report revealed that in cultured cell lines, SGMS1 localizes in Golgi apparatus while SGMS2 localizes in the plasma membrane [28]. Thus, the results of this previous report suggest that SMs synthesized by SGMS1 can be easily incorporated into membranous replication complexes. As for SGMS2, we found that HCV infection significantly increased the expression of SGMS2, although the relationship between SGMS2 and HCV replication was hardly seen in this study. The relationship between SGMS2 and HCV propagation, thus, is an issue that should be elucidated in future studies.

We also demonstrated in this study that reduction of SM molecular species by NA808, a hepatotropic SPT inhibitor with little immunosuppressive activity, inhibits HCV replication in humanized chimeric mice regardless of viral genotype (Figure 4). Notably, treatment with NA808 (5 mg/kg) restored SM and ceramide levels in the liver to the levels observed in uninfected chimeric mice (Figure 5). Apparently, a slight reduction in SM had a significant influence on HCV, indicating that SM plays an important role in the HCV life cycle. SM is required for many viral processes in host-pathogen interactions [29–31]. For instance, viral envelopes of human immunodeficiency virus type 1 (HIV-1) and herpes simplex virus (HSV) are enriched with SM, which is necessary for efficient virus infectivity [32,33]. With regard to HCV, in addition to efficient virus infectivity [34], SM is present in the raft domain, which serves as a site of virus replication, together with other sphingolipids and cholesterol [6]. Moreover, SM is a component of VLDL whose assembly component and pathway is required for HCV morphogenesis and secretion [34,35]. The above-mentioned observations suggest that SM plays a multifaceted role in the HCV life cycle; therefore, SM is likely to be a good therapeutic target.

HCV is thought to replicate in a specialized compartment characterized as a DRM (designated as the membranous replication complex) [6]. SM, cholesterol, and phosphatidylinositol (PI) are thought to be the lipids that make up the membranous replication complex. With regard to PI, several siRNA screening have recently identified type III phosphatidylinositol 4-kinases (PI4K) as crucial host factors for HCV replication [36–39]. In HCV replicon containing cells, PI4P distribution is altered and enriched in the membranous replication complex by PI4KIIIα synthesis. Although the ability of PI to influence membrane bending and regulate intracellular processes (e.g. vesicle fusion, budding, and sorting) has been reported, the role of PI4P in the formation of the membranous replication complex remains to be elucidated. SM and cholesterol organize the solid membrane characterized as the DRM, where HCV replicates [6]. In fact, we and other groups demonstrated that reduction of SM and cholesterol suppressed HCV replication [7,9,12,40]. We performed the immunofluorescent analysis using lysenin. However, lysenin did not co-localize with NS4B protein. To date, it has been reported that lysenin-binding to SM is increased in the form of SM clusters, and that glycosphingolipids hinder lysein-binding to SM [41] Lipid rafts form of HCV replication complex do not have the characters of lysenin-binding to SM.

Further, the role of SM is not only to act as a constituent of the membranous replication complex, but also to bind and activate RdRp [7,8]. In this study, to gain further insight into the HCV membranous replication complex, we attempted to analyze which SM molecular species comprise the membranous replication complex, given that the diversity of molecular species is believed to be responsible for the physiochemical properties of the biomembrane [42] (Figure 6). We found that the composition ratio of SM molecular species observed in this study was quite different between the whole cell and DRM fractions. Further, to identify whether these SM molecular species contribute to HCV replication, we conducted rescue experiments using HCV replicon-containing cells (carrying intact RdRp and active membranous replication complexes) in which each SM molecular species was extrinsically added to replicon cells treated with NA808. However, in this experiment, addition of SM caused cell death. Therefore, we used digitonin-permeabilized semi-intact replicon cells, which enabled us to deliver the extrinsically added SM molecular species directly to the cytosol without catalytic effect and permitted monitoring of intact RdRp and replication complexes. We demonstrated that the specific endogenous SM molecular species (*d*18:1-16:0 and *d*18:1-24:0) enhance HCV-RNA replication, these species being consistent with the two SM molecular species which mainly constitute the DRM. Collectively, these results suggest that the HCV replication complex characterized as DRM is the specialized compartment that is composed of SM molecular species. These findings will provide new insights into the formation of the HCV replication complex and the involvement of host lipids in the HCV life cycle.

Materials and Methods

Ethics statement

This study was carried out in strict accordance with both the Guidelines for Animal Experimentation of the Japanese Association for Laboratory Animal Science and the recommendations in the Guide for the Care and Use of Laboratory Animals of the National Institutes of Health. All protocols were approved by the ethics committee of Tokyo Metropolitan Institute of Medical

Science. The patient with HCV infection who provided the serum samples gave written informed consent before blood collection.

Cells

The HCV subgenomic replicon cells FLR3-1 (genotype 1b, Con-1) was cultured at 37°C in Dulbecco's modified Eagle's medium GlutaMax-I (Invitrogen, Carlsbad, CA, USA) supplemented with 10% fetal bovine serum (FBS) and 0.5 mg/mL G418. HuH-7 K4 cells (cured of HCV by IFN treatment) and the JFH/K4 cells persistently infected with the HCV JFH-1 strain were maintained in DMEM containing 10% FCS and 0.1 mg/mL penicillin and streptomycin sulfate. MH-14 cells were grown in Dulbecco's modified Eagle's medium supplemented with 10% fetal bovine serum, 100 U/mL nonessential amino acids, 0.1 mg/mL penicillin and streptomycin sulfate, and 0.5 mg/mL G418.

siRNA assay

siCONTROL, siSGMS1, and siSGMS2 were purchased from Dharmacon RNA Technologies (Lafayette, CO, USA). The siCONTROL Non-Targeting siRNA #3 was used as the negative control siRNA. We used siRNAs against the HCV genome (siE-R7) [16]. The chemically synthesized siRNAs were transfected into cells using Lipofectamine RNAiMAX (Invitrogen) and Opti-MEM (Invitrogen) by reverse-transfection. Cells were characterized at 96 h after transfection.

Serine palmitoyltransferase activity

We assessed SPT activity in the liver as previously described, with minor modifications [43]. Briefly, frozen cells were homogenized in HEPES buffer (10 mM HEPES, 2 mM sucrose monolaurate, and 0.25 M sucrose, pH 7.4), and homogenates were centrifuged at 10,000×*g* for 20 min. From the resulting supernatant, samples containing 200 µg protein were assayed for SPT activity using [^{14}C]-serine and palmitoyl-CoA (Sigma-Aldrich, St. Louis, MO, USA) as substrates.

Proliferation assay

Human peripheral blood cells (AllCells, Emeryville, CA, USA) were plated onto 96-well plates and treated with phytohemagglutinin with or without immunosuppressant reagents. After 2 days of stimulation, [^{3}H]-thymidine-containing growth medium was added, and the cultures were incubated for another 18 h. T-cell proliferation was assessed by comparing the level of thymidine incorporation to that in the stimulated control.

Anti-hepatitis C virus assay in Huh-7 cells harboring subgenomic replicons

Replication was determined after 72 h with a Bright-Glo luciferase assay kit (Promega, Madison, WI, USA). The viability of replicon cells was determined using a cell counting kit (Dojindo, Kumamoto, Japan) according to the manufacturer's instructions.

Western blot analysis

Cells were resuspended in lysis buffer (10 mM Tris, pH 7.4 containing 1% SDS, 0.5% Nonidet P-40, 150 mM NaCl, 0.5 mM EDTA, and 1 mM dithiothreitol). Ten micrograms of the resulting protein sample were electrophoresed on a 10% sodium dodecyl sulfate-polyacrylamide gel and subsequently transferred to a polyvinylidene difluoride membrane (Immobilon-P; Millipore, Billerica, MA, USA). HCV nonstructural protein 3 (NS3) and nonstructural 5B polymerase (RdRp) were detected with rabbit anti-NS3 polyclonal antibody (R212) and mouse anti-RdRp monoclonal antibody (5B-14) prepared in our laboratory. β-Actin was detected with anti-β-actin monoclonal antibody (Sigma-Aldrich).

Immunofluorescent staining of hepatitis C virus replicon cells

After treatment with 25 nM NA808 for 96 h, FLR3-1 cells were probed with anti-NS3 polyclonal antibody (R212; the primary antibody). Next, an anti-rabbit IgG-Alexa 488 conjugate (Invitrogen) was applied as the secondary antibody.

Thin-layer chromatography analysis

Thin-layer chromatography (TLC) analysis was performed as described previously [9]. Briefly, cells were incubated with [^{14}C]-serine in Opti-MEM (Invitrogen). Cells extracts were obtained using the Bligh & Dyer method [44] and were spotted onto Silica Gel 60 TLC plates (Merck, Darmstadt, Germany) for separation. Radioactive spots were detected using a BAS 2000 system (Fuji Film, Kanagawa, Japan).

Membrane flotation assay

Cells were lysed in TNE buffer (25 mM Tris-HCl, 150 mM NaCl, 1 mM EDTA) and passed 20 times through a 25-gauge needle. Nuclei and unbroken cells were removed by centrifugation at 1,000×*g* for 5 min. After ensuring that the amount of total protein was equivalent across all samples, cell lysates were treated with 1% Triton on ice for 30 min and then subjected to a sucrose gradient (10%, 30%, and 40%). The sucrose gradient was centrifuged at 247,220×*g* in a Beckman SW41 Ti rotor (Beckman Coulter Inc., Brea, CA, USA) for 14 h at 4°C. Fractions (1 mL) were collected from the top of the gradient.

Infection of mice with hepatitis C virus genotypes 1a and 2a

Chimeric mice infected with HCV were prepared as previously described [45]. Briefly, approximately 40 days after the transplantation procedure, mice were intravenously injected with 5×10^5 copies/mouse of HCG9 (genotype 1a) or HCR24 (genotype 2a) that had been collected from patient serum.

Quantification of HCV RNA by real-time polymerase chain reaction

Total RNA was purified from 1 µL of chimeric mouse serum using SepaGene RV-R (Sanko Junyaku Co. Ltd., Tokyo, Japan) and from liver tissue using Isogene (Nippon Gene Co. Ltd., Tokyo, Japan). HCV RNA was quantified by quantitative real-time polymerase chain reaction (PCR) using previously reported techniques [9]. For serum, this technique has a lower limit of detection of 4000 copies/mL. Therefore, samples in which HCV RNA was undetectable were assigned this minimum value.

Quantification of HCV core protein by ELISA

Liver specimens were homogenized in TNE buffer. Aliquots of 5 µg of total protein were assayed for core protein levels with an Ortho HCV core protein ELISA kit (Eiken Chemical, Tokyo, Japan).

Indirect immunofluorescence analysis

The primary antibody for immunofluorescence analysis of liver sections was anti-HCV core protein monoclonal antibody (5E3) [46]. Monoclonal antibody labeling was followed by staining with anti-mouse IgG Alexa-488. The nuclei were stained using 4′,6-diamidino-2-phenylindole (DAPI).

Gene expression analysis

To measure mRNA levels, total RNA samples were extracted from the mouse livers and cDNA was synthesized using a High-Capacity cDNA Reverse Transcription Kit (Applied Biosystems, Foster City, CA, USA). The cDNA solution was assessed by quantitative PCR performed with TaqMan Gene Expression Assays (Applied Biosystems) and an ABI 7700 Sequence Detection System (Applied Biosystems).

Quantification of SM and ceramide in liver

We quantified liver SM and ceramide levels using a mass spectrometer (MS). Electrospray ionization (ESI)-MS analysis was performed using a 4000Q TRAP quadrupole-linear ion trap hybrid MS (AB SCIEX, Foster City, CA, USA) with an UltiMate 3000 nano/cap/micro-liquid chromatography system (Dionex Corporation, Sunnyvale, CA, USA) combined with an HTS PAL autosampler (CTC Analytics AG, Zwingen, Switzerland). The total lipid fractions expected to contain SM and ceramide, were subjected directly to flow injection and were selectively analyzed by neutral loss scanning of 60 Da (HCO_2+CH_3) from SM $[M+HCOO]^-$ in the negative ion mode, and multiple-reaction monitoring using a combination of ceramide $[Cer-H_2O+H]^+$ and the product (long-chain base) $[LCB-H_2O+H]^+$ in the positive ion mode [47,48]. The mobile phase composition was acetonitrile:methanol:water at 6:7:2 (0.1% ammonium formate, pH 6.8) and a flow rate of 10 μL/min. The typical injection volume was 3 μL of total lipids, normalized by protein content.

LC/ESI-MS analysis was performed using quadrupole/time of flight (Q-TOF) micro with an ACQUITY UPLC system (Waters Corporation, Milford, MA, USA) in the negative ion mode and an Agilent 6230 with an Agilent 1290 Infinity LC system (Agilent Technologies, Inc., Loveland, CO, USA) in the positive ion mode. Reversed-phase LC separation was achieved using an ACQUITY UPLC BEH column (150 mm×1.0 mm i.d., Waters Corporation) at 45°C. The mobile phase was acetonitrile:methanol:water at 19:19:2 (0.1% formic acid+0.028% ammonia) (A) and isopropanol (0.1% formic acid+0.028% ammonia) (B), and the composition was produced by mixing these solvents. The gradient consisted of holding A:B at 90:10 for 7.5 min, then linearly converting to A:B at 70:30 for 32.5 min, and then linearly converting to A:B at 40:60 for 50 min. The detailed procedure for LC/ESI-MS was described previously [49,50].

Separation of SM molecular species by HPLC

Bovine milk or brain SM (Avanti Polar Lipids. Inc., Alabaster, AL, USA) was dissolved in chloroform:methanol (2:1), then separated according to molecular species by reversed-phase HPLC. The *d*18:1-16:0, 22:0, and 24:0 molecular species of SM were isolated from bovine milk SM, while the *d*18:1-24:0 and 24:1 molecular species were isolated from brain SM. Bovine milk and brain SM were then separated on Senshu PAK ODS (C18) columns (Senshu Scientific Co., Ltd., Tokyo, Japan) using methanol as the eluting solvent at a flow rate of 1 mL/min. The fatty acid compositions of the purified fractions were analyzed by LC/ESI-MS. The amount of SM in each fraction was quantified using an SM assay kit (Cayman Chemical, Ann Arbor, MI, USA). We confirmed that the purity of each molecular species was approximately 90% without *d*18:1-24:1 (about 70%) (data not shown).

In vitro HCV transcription

In vitro HCV transcription was performed as previously described [8].

SM binding assay using ELISA

An SM binding assay was performed as previously described [8] using rabbit anti-HCV RdRp sera (1:5000) and an HRP-conjugated anti-rabbit IgG antibody (1:5000). Optical density at 450 nm (OD_{450}) was measured on a Spectra Max 190 spectrophotometer (Molecular Devices, Sunnyvale, CA, USA) using the TMB Liquid Substrate System (Sigma).

RNA replication assays in permeabilized replicon cells

The analysis using digitonin-permeabilized replicon cells was performed as previously described [20] with minor modifications. Briefly, MH-14 cells of about 80% confluency were pre-cultured for 2 h in complete Dulbecco's modified Eagle's medium containing 5 μg/mL actinomycin D (Nacalai Tesque, Kyoto, Japan), then washed with cold buffer B (20 mM HEPES-KOH (pH 7.7 at 27°C), 110 mM potassium acetate, 2 mM magnesium acetate, 1 mM EGTA, and 2 mM dithiothreitol). The cells were permeabilized by incubation in buffer B containing 50 μg/mL digitonin for 5 min at 27°C, and the reaction was stopped by washing twice with cold buffer B. The permeabilized cells were then incubated for 4 h at 27°C in the reaction mixture with or without each lipid. The reaction mixture consisted of 2 mM manganese(II) chloride, 1 mg/mL acetylated bovine serum albumin (Nacalai Tesque), 5 mM phosphocreatine (Sigma), 20 units/mL creatine phosphokinase (Sigma), 50 μg/mL actinomycin D, and 500 μM each of ATP, CTP, GTP, and UTP (Roche Diagnostics, Basel, Switzerland) in buffer B (pH 7.7). Total RNA was purified by the acid guanidinium-phenol-chloroform method. In this assay, considering that the estimated SM content in human hepatocytes is 3–4 nmol/mg protein, as demonstrated by MS analysis (**Figure S10**), the amount of SM we added in the replicase assay was 0.3–1 μM. (i.e. 0.03–0.3 nmol/0.3 mL/0.1 mg protein/12 well; the reaction volume in the replicase assay was 0.3 mL/12 wells and each well of the 12 well cell culture plates contained approximately 0.1 mg protein.)

Statistical analysis

Statistical analysis was performed using the Student's *t*-test equipped with Excel 2008 (Microsoft, Redmond, WA, USA). To measure the strength of the association, Pearson correlation coefficient was calculated using Excel 2008. A p-value<0.05 was considered statistically significant.

Supporting Information

Figure S1 Impacts of HBV infection on expression of sphingomyelin (SM) biosynthesis genes. mRNA expression of *SGMS1* and *SGMS2* genes (encoding SM synthases 1 and 2, respectively) in uninfected (white) and infected (black) chimeric mice (n = 5 per group).
(JPG)

Figure S2 Effect of HCV infection in cultured cells. Comparison of the relative amounts of SM, as measured by MS analysis, in mock-infected (HuH-7 K4 cells) (white) and HCV (JFH-1)-infected cells (JFH/K4 cells) (black) (n = 1 per group).
(JPG)

Figure S3 The expression of HCV core protein in HCV-infected chimeric mice. Histological analysis using immunohistochemical labeling of HCV core protein.
(JPG)

Figure S4 Effects of NA808 on HCV-infected chimeric mice. (**A**) Average body weight of mice during treatment. (**B**) Average human albumin concentrations in the sera of mice during

treatment. (**C**) Histological analysis using H&E staining and immunofluorescent labeling of human albumin (red). In all cases, error bars indicate SDs.
(JPG)

Figure S5 Concentrations of NA808 in chimeric mice receiving NA808 treatment. Concentration of NA808 in the liver (gray) and serum (black) of chimeric mice treated with 5 mg/kg or 10 mg/kg NA808. Stars indicate that NA808 level was not detected.
(JPG)

Figure S6 Sphingomyelin (SM) levels in the serum of chimeric mice receiving NA808 treatment. SM levels in the serum of chimeric mice (n = 3 per group) that were uninfected (HCV−), or infected (HCV+) but untreated or treated with 5 or 10 mg/kg NA808. Error bars indicate SDs.
(JPG)

Figure S7 Effects of NA808 on associations between the HCV nonstructural 5B polymerase (RdRp) and sphingomyelin (SM). (**A**) Comparison of SDS-PAGE and TLC results for replicon cells receiving no treatment (Control) or NA808 treatment (NA808). NA808 dosage was 2.5 nM (for TLC) or 25 nM (for SDS-PAGE). (**B**) Relative band intensities of RdRp and NS3 in detergent-resistant membrane (DRM) fractions from cells receiving no treatment (Control) or 25 nM NA808 treatment (NA808). (**C**) Relative band intensities of SM in DRM fractions from cells receiving no treatment (Control) or 2.5 nM NA808 treatment (NA808).
(JPG)

Figure S8 Composition ratio of SM molecular species in whole cells and DRM fraction of uninfected cells.
(JPG)

Figure S9 Effect of NS3 protease inhibitor on SM molecular species in the DRM fractions of subgenomic replicon cells. (A) Effect of NS3 protease inhibitor (VX950) on HCV replication (dark grey bars) and cell viability (light grey bars) in FLR3-1 replicon-containing cells. Error bars indicate SD. (B) Effect of NS3 protease inhibitor (VX950; 3 μM) on SM molecular species of DRM fractions of FLR 3-1 replicon-containing cells. Error bars indicate SDs.
(JPG)

Figure S10 The estimated SM content in human hepatocytes. Left bar (white) indicates the intensity of SM internal standard (SM d18:0-12:0; 1 nmol) by mass spectrometer. Right bar indicates the intensity of 1 mg protein of human hepatocyte (HuH-7 K4).
(JPG)

Table S1 Distribution of radioactivity in tissues after a single intravenous administration of [^{14}C] NA808 at 2 mg/kg to non-fasting male rats.
(PDF)

Table S2 Treatment administration for HCV-infected chimeric mice. Administration of reagents was started at day 0. The amount of NA808 was adjusted according to the body weight of the mice. Dose began at 5 mg/kg or 10 mg/kg and was reduced by half at each 10% reduction in body weight (half circle). At 20% reduction, administration was discontinued. Open circle indicates each manipulation was performed as required.
(PDF)

Text S1 Materials and methods for supporting information. Methods for "Infection of chimeric mice with hepatitis B virus", "Quantification of human albumin", "Histological staining and indirect immunofluorescence analysis", and "Quantification of sphingomyelin (SM) in serum" are described.
(DOCX)

Acknowledgments

We are very grateful to Dr. Makoto Hijikata of the Department of Viral Oncology, Institute for Virus Research, Kyoto University for his technical support. We thank Isao Maruyama and Hiroshi Yokomichi of PhoenixBio Co., Ltd. for maintenance of and technical assistance with the chimeric mice.

Author Contributions

Conceived and designed the experiments: M. Kohara. Wrote the paper: Y. Hirata. Y. Hirata performed the experiment of chimeric mice and HCV-infected cells. K. Ikeda, M. Ohta, T. Soga, and R. Taguchi performed lipid analysis by MS spectrometry. M. Sudoh, A. Katsume, and Y. Aoki evaluated the antiviral effects of NA808, K. Okano and K. Ozeki examined the tissue distribution of NA808. K. Kawasaki and T. Tsukuda synthesized derivatives from natural compounds. Y. Tokunaga, Y. Tobita, T. Umehara, and S. Sekiguchi performed some experiments on the chimeric mice. L. Weng and T. Toyoda conducted the experiments on the interaction between RdRp and SM. M. Kohara and Y. Hirata performed data analysis on the chimeric mice and cells. K. Ikeda, M. Ohta, T. Soga, and R. Taguchi performed data analysis on the result of MS spectrometry. A. Suzuki, K. Shimotohno, and M. Nishijima provided tools and expert information.

References

1. Wenk MR (2006) Lipidomics of host-pathogen interactions. FEBS Lett 580: 5541–5551.
2. Brown DA, Rose JK (1992) Sorting of GPI-anchored proteins to glycolipid-enriched membrane subdomains during transport to the apical cell surface. Cell 68: 533–544.
3. Simons K, Toomre D (2000) Lipid rafts and signal transduction. Nat Rev Mol Cell Biol 1: 31–39.
4. van der Meer-Janssen YP, van Galen J, Batenburg JJ, Helms JB (2010) Lipids in host-pathogen interactions: pathogens exploit the complexity of the host cell lipidome. Prog Lipid Res 49: 1–26.
5. Aizaki H, Lee KJ, Sung VM, Ishiko H, Lai MM (2004) Characterization of the hepatitis C virus RNA replication complex associated with lipid rafts. Virology 324: 450–461.
6. Shi ST, Lee KJ, Aizaki H, Hwang SB, Lai MM (2003) Hepatitis C virus RNA replication occurs on a detergent-resistant membrane that cofractionates with caveolin-2. J Virol 77: 4160–4168.
7. Sakamoto H, Okamoto K, Aoki M, Kato H, Katsume A, et al. (2005) Host sphingolipid biosynthesis as a target for hepatitis C virus therapy. Nat Chem Biol 1: 333–337.
8. Weng L, Hirata Y, Arai M, Kohara M, Wakita T, et al. (2010) Sphingomyelin activates hepatitis C virus RNA polymerase in a genotype-specific manner. J Virol 84: 11761–11770.
9. Umehara T, Sudoh M, Yasui F, Matsuda C, Hayashi Y, et al. (2006) Serine palmitoyltransferase inhibitor suppresses HCV replication in a mouse model. Biochem Biophys Res Commun 346: 67–73.
10. Kapadia SB, Chisari FV (2005) Hepatitis C virus RNA replication is regulated by host geranylgeranylation and fatty acids. Proc Natl Acad Sci U S A 102: 2561–2566.
11. Su AI, Pezacki JP, Wodicka L, Brideau AD, Supekova L, et al. (2002) Genomic analysis of the host response to hepatitis C virus infection. Proc Natl Acad Sci U S A 99: 15669–15674.
12. Takano T, Tsukiyama-Kohara K, Hayashi M, Hirata Y, Satoh M, et al. (2011) Augmentation of DHCR24 expression by hepatitis C virus infection facilitates viral replication in hepatocytes. J Hepatol 55: 512–521.
13. Tateno C, Yoshizane Y, Saito N, Kataoka M, Utoh R, et al. (2004) Near completely humanized liver in mice shows human-type metabolic responses to drugs. Am J Pathol 165: 901–912.
14. Mercer DF, Schiller DE, Elliott JF, Douglas DN, Hao C, et al. (2001) Hepatitis C virus replication in mice with chimeric human livers. Nat Med 7: 927–933.

15. Valsecchi M, Mauri L, Casellato R, Prioni S, Loberto N, et al. (2007) Ceramide and sphingomyelin species of fibroblasts and neurons in culture. J Lipid Res 48: 417–424.
16. Watanabe T, Sudoh M, Miyagishi M, Akashi H, Arai M, et al. (2006) Intracellular-diced dsRNA has enhanced efficacy for silencing HCV RNA and overcomes variation in the viral genotype. Gene Ther 13: 883–892.
17. Fujita T, Inoue K, Yamamoto S, Ikumoto T, Sasaki S, et al. (1994) Fungal metabolites. Part 11. A potent immunosuppressive activity found in Isaria sinclairii metabolite. J Antibiot (Tokyo) 47: 208–215.
18. Miyake Y, Kozutsumi Y, Nakamura S, Fujita T, Kawasaki T (1995) Serine palmitoyltransferase is the primary target of a sphingosine-like immunosuppressant, ISP-1/myriocin. Biochem Biophys Res Commun 211: 396–403.
19. Park TS, Panek RL, Mueller SB, Hanselman JC, Rosebury WS, et al. (2004) Inhibition of sphingomyelin synthesis reduces atherogenesis in apolipoprotein E-knockout mice. Circulation 110: 3465–3471.
20. Miyanari Y, Hijikata M, Yamaji M, Hosaka M, Takahashi H, et al. (2003) Hepatitis C virus non-structural proteins in the probable membranous compartment function in viral genome replication. J Biol Chem 278: 50301–50308.
21. Diamond DL, Jacobs JM, Paeper B, Proll SC, Gritsenko MA, et al. (2007) Proteomic profiling of human liver biopsies: hepatitis C virus-induced fibrosis and mitochondrial dysfunction. Hepatology 46: 649–657.
22. Tardif KD, Mori K, Siddiqui A (2002) Hepatitis C virus subgenomic replicons induce endoplasmic reticulum stress activating an intracellular signaling pathway. J Virol 76: 7453–7459.
23. Pettus BJ, Chalfant CE, Hannun YA (2002) Ceramide in apoptosis: an overview and current perspectives. Biochim Biophys Acta 1585: 114–125.
24. Tepper AD, Ruurs P, Wiedmer T, Sims PJ, Borst J, et al. (2000) Sphingomyelin hydrolysis to ceramide during the execution phase of apoptosis results from phospholipid scrambling and alters cell-surface morphology. J Cell Biol 150: 155–164.
25. Liu YY, Han TY, Giuliano AE, Hansen N, Cabot MC (2000) Uncoupling ceramide glycosylation by transfection of glucosylceramide synthase antisense reverses adriamycin resistance. J Biol Chem 275: 7138–7143.
26. Taguchi Y, Kondo T, Watanabe M, Miyaji M, Umehara H, et al. (2004) Interleukin-2-induced survival of natural killer (NK) cells involving phosphatidylinositol-3 kinase-dependent reduction of ceramide through acid sphingomyelinase, sphingomyelin synthase, and glucosylceramide synthase. Blood 104: 3285–3293.
27. Diamond DL, Syder AJ, Jacobs JM, Sorensen CM, Walters KA, et al. (2010) Temporal proteome and lipidome profiles reveal hepatitis C virus-associated reprogramming of hepatocellular metabolism and bioenergetics. PLoS Pathog 6: e1000719.
28. Huitema K, van den Dikkenberg J, Brouwers JF, Holthuis JC (2004) Identification of a family of animal sphingomyelin synthases. EMBO J 23: 33–44.
29. Merrill AH, Jr., Schmelz EM, Dillehay DL, Spiegel S, Shayman JA, et al. (1997) Sphingolipids–the enigmatic lipid class: biochemistry, physiology, and pathophysiology. Toxicol Appl Pharmacol 142: 208–225.
30. Huwiler A, Kolter T, Pfeilschifter J, Sandhoff K (2000) Physiology and pathophysiology of sphingolipid metabolism and signaling. Biochim Biophys Acta 1485: 63–99.
31. Hannun YA, Luberto C, Argraves KM (2001) Enzymes of sphingolipid metabolism: from modular to integrative signaling. Biochemistry 40: 4893–4903.
32. van Genderen IL, Brandimarti R, Torrisi MR, Campadelli G, van Meer G (1994) The phospholipid composition of extracellular herpes simplex virions differs from that of host cell nuclei. Virology 200: 831–836.
33. Brugger B, Glass B, Haberkant P, Leibrecht I, Wieland FT, et al. (2006) The HIV lipidome: a raft with an unusual composition. Proc Natl Acad Sci U S A 103: 2641–2646.
34. Aizaki H, Morikawa K, Fukasawa M, Hara H, Inoue Y, et al. (2008) Critical role of virion-associated cholesterol and sphingolipid in hepatitis C virus infection. J Virol 82: 5715–5724.
35. Syed GH, Amako Y, Siddiqui A (2010) Hepatitis C virus hijacks host lipid metabolism. Trends Endocrinol Metab 21: 33–40.
36. Berger KL, Cooper JD, Heaton NS, Yoon R, Oakland TE, et al. (2009) Roles for endocytic trafficking and phosphatidylinositol 4-kinase III alpha in hepatitis C virus replication. Proc Natl Acad Sci U S A 106: 7577–7582.
37. Borawski J, Troke P, Puyang X, Gibaja V, Zhao S, et al. (2009) Class III phosphatidylinositol 4-kinase alpha and beta are novel host factor regulators of hepatitis C virus replication. J Virol 83: 10058–10074.
38. Tai AW, Benita Y, Peng LF, Kim SS, Sakamoto N, et al. (2009) A functional genomic screen identifies cellular cofactors of hepatitis C virus replication. Cell Host Microbe 5: 298–307.
39. Vaillancourt FH, Pilote L, Cartier M, Lippens J, Liuzzi M, et al. (2009) Identification of a lipid kinase as a host factor involved in hepatitis C virus RNA replication. Virology 387: 5–10.
40. Amemiya F, Maekawa S, Itakura Y, Kanayama A, Matsui A, et al. (2008) Targeting lipid metabolism in the treatment of hepatitis C virus infection. J Infect Dis 197: 361–370.
41. Ishitsuka R, Sato SB, Kobayashi T (2005) Imaging lipid rafts. J Biochem 137: 249–254.
42. Ramstedt B, Slotte JP (2002) Membrane properties of sphingomyelins. FEBS Lett 531: 33–37.
43. He Q, Suzuki H, Sharma N, Sharma RP (2006) Ceramide synthase inhibition by fumonisin B1 treatment activates sphingolipid-metabolizing systems in mouse liver. Toxicol Sci 94: 388–397.
44. Bligh EG, Dyer WJ (1959) A rapid method of total lipid extraction and purification. Can J Biochem Physiol 37: 911–917.
45. Inoue K, Umehara T, Ruegg UT, Yasui F, Watanabe T, et al. (2007) Evaluation of a cyclophilin inhibitor in hepatitis C virus-infected chimeric mice in vivo. Hepatology 45: 921–928.
46. Kashiwakuma T, Hasegawa A, Kajita T, Takata A, Mori H, et al. (1996) Detection of hepatitis C virus specific core protein in serum of patients by a sensitive fluorescence enzyme immunoassay (FEIA). J Immunol Methods 190: 79–89.
47. Ikeda K, Shimizu T, Taguchi R (2008) Targeted analysis of ganglioside and sulfatide molecular species by LC/ESI-MS/MS with theoretically expanded multiple reaction monitoring. J Lipid Res 49: 2678–2689.
48. Taguchi R, Nishijima M, Shimizu T (2007) Basic analytical systems for lipidomics by mass spectrometry in Japan. Methods Enzymol 432: 185–211.
49. Ikeda K, Oike Y, Shimizu T, Taguchi R (2009) Global analysis of triacylglycerols including oxidized molecular species by reverse-phase high resolution LC/ESI-QTOF MS/MS. J Chromatogr B Analyt Technol Biomed Life Sci 877: 2639–2647.
50. Ikeda K, Mutoh M, Teraoka N, Nakanishi H, Wakabayashi K, et al. (2011) Increase of oxidant-related triglycerides and phosphatidylcholines in serum and small intestinal mucosa during development of intestinal polyp formation in Min mice. Cancer Sci 102: 79–87.

PLOS | ONE

Comprehensive miRNA Expression Analysis in Peripheral Blood Can Diagnose Liver Disease

Yoshiki Murakami[1]*, Hidenori Toyoda[2], Toshihito Tanahashi[3], Junko Tanaka[4], Takashi Kumada[2], Yusuke Yoshioka[5], Nobuyoshi Kosaka[5], Takahiro Ochiya[5], Y-h Taguchi[6]

1 Department of Hepatology, Graduate School of Medicine, Osaka City University, Osaka, Japan, **2** Department of Gastroenterology, Ogaki Municipal Hospital, Ogaki, Japan, **3** Department of Medical Pharmaceutics, Kobe Pharmaceutical University, Kobe, Japan, **4** Department of Epidemiology, Infectious Disease Control and Prevention, Hiroshima University Graduate School of Biomedical Sciences, Hiroshima, Japan, **5** Division of Molecular and Cellular Medicine, National Cancer Center Research Institute, Tokyo, Japan, **6** Department of Physics, Chuo University, Tokyo, Japan

Abstract

Background: miRNAs circulating in the blood in a cell-free form have been acknowledged for their potential as readily accessible disease markers. Presently, histological examination is the golden standard for diagnosing and grading liver disease, therefore non-invasive options are desirable. Here, we investigated if miRNA expression profile in exosome rich fractionated serum could be useful for determining the disease parameters in patients with chronic hepatitis C (CHC).

Methodology: Exosome rich fractionated RNA was extracted from the serum of 64 CHC and 24 controls with normal liver (NL). Extracted RNA was subjected to miRNA profiling by microarray and real-time qPCR analysis. The miRNA expression profiles from 4 chronic hepatitis B (CHB) and 12 non alcoholic steatohepatitis (NASH) patients were also established. The resulting miRNA expression was compared to the stage or grade of CHC determined by blood examination and histological inspection.

Principal Findings: miRNAs implicated in chronic liver disease and inflammation showed expression profiles that differed from those in NL and varied among the types and grades of liver diseases. Using the expression patterns of nine miRNAs, we classified CHC and NL with 96.59% accuracy. Additionally, we could link miRNA expression pattern with liver fibrosis stage and grade of liver inflammation in CHC. In particular, the miRNA expression pattern for early fibrotic stage differed greatly from that observed in high inflammation grades.

Conclusions: We demonstrated that miRNA expression pattern in exosome rich fractionated serum shows a high potential as a biomarker for diagnosing the grade and stage of liver diseases.

Citation: Murakami Y, Toyoda H, Tanahashi T, Tanaka J, Kumada T, et al. (2012) Comprehensive miRNA Expression Analysis in Peripheral Blood Can Diagnose Liver Disease. PLoS ONE 7(10): e48366. doi:10.1371/journal.pone.0048366

Editor: Xiao-Ping Miao, MOE Key Laboratory of Environment and Health, School of Public Health, Tongji Medical College, Huazhong University of Science and Technology, China

Received May 17, 2012; **Accepted** September 24, 2012; **Published** October 31, 2012

Funding: Y.M, J.T, and T.K. were financially supported by the Ministry of Health, Labour and Welfare of Japan (H22-general-008)and Y.M, J.T, T.K, and Y.T received Grants-in-Aid for scientific research from the Ministry of Education, Culture, Sports, Science and Technology (22590727). The funders had no role in study design, data collection and analysis, decision to publish, or preparation of the manuscript.

Competing Interests: The authors have declared that no competing interests exist.

* E-mail: m2079633@med.osaka-cu.ac.jp

Introduction

MicroRNAs (miRNAs) are a gene family that is evolutionarily conserved and have important roles in the control of many biological processes, such as cellular development, differentiation, proliferation, apoptosis, and metabolism [1]. Aberrant expression of miRNAs in liver tissue has been implicated in the progression of liver fibrosis, and hepatocarcinogenesis [2,3,4]. Recently, two independent groups showed that miR-122 plays a critical role in the maintenance of liver homeostasis and anti-tumor formation [5,6].

Exosome in one of the endoplasmic reticulum carries mRNAs and miRNAs [7]. Recently, it has become clear that exosome perform intercellular signaling through miRNA. miRNAs are released through a ceramide-dependent secretory machinery and are then transferred and become functional in the recipient cells [8]. In a prior study using human blood and cultured cells, several miRNAs were selectively packaged into microvesicle (MV) and actively secreted [9]. In another study, miRNAs originating from EBV was transported by exosome and then participated in the immune response of host cells [10]. In HCC cells as well, this type of exosome-mediated miRNA transfer is an important mechanism of intercellular communication [11].

It has also become clear that exosome can adjust to immune function, control infection or carry the virus itself. Exosomes of T, B and dendritic immune cells contain a repertoire of miRNAs that differ from that of their parent cells [12,13]. Exosomes released from nasopharyngeal carcinoma cells harboring latent EBV were shown to contain LMP1, signal transduction molecules, and virus-encoded miRNAs [14]. Retroviruses evade adaptive immune responses by using nonviral or host exosome biogenesis pathways to form infectious particles and as a mode of infection [15].

Recent evidence has shown that the expression patterns of serum or plasma miRNAs are altered in several diseases, in particular heart disease, sepsis, malignancies, and autoimmune diseases (reviewed in [16]). Discoveries such as this is encouraging and has propelled further research leading to the hypothesis that circulating miRNAs are detectable in serum and plasma in a form sufficiently stable to serve as biomarkers [17,18]. One such example is that tumour-associated miRNAs were found in the serum of diffuse large B-cell lymphoma patients [19]. In other examples, serum levels of miR-34a and miR-122 were associated with histological disease severity in patients with CHC or non-alcoholic fatty-liver disease (NAFLD) [20]. In fact, the serum level of miR-122 strongly correlates with serum ALT activity and with necro-inflammatory activity in patients with CHC and elevated ALT levels. However, there seems to be no significant correlation between fibrosis stage and functional capacity of the liver [21]. The expression levels of miR-122 and miR-194 correlated negatively with age in patients with CHB and HBV associated acute-on-chronic liver failure [22]. The expression level of miR-122 in serum was found to be closely related to non drug-induced acute liver injury [23]. Based on the above, it comes as no surprise that recently, the expression profile from extracellular miRNA is being used clinically to diagnose various diseases.

Here, in order to obtain data with high resolution that is reproducible, we extracted MVs from serum using exoquick and then performed a comprehensive microarray analysis. We attempted to diagnose HCV infection, and ascertain the degree of liver inflammation and fibrosis stage using exosome-rich fractioned miRNA. In short, we investigate if serum-derived miRNAs had the potential to serve as non-invasive bio-markers for various liver diseases.

Results

Reproducible Gene-analysis Using Microarray

In microarray experiments, serum analysis is comparatively easy; however, the downside is that the accuracy and reproducibility of the results are usually not satisfactory. To circumvent this drawback, we devised a procedure that would give us higher accuracy and reproducibility. Serum samples from NL subjects were prepared and divided into two groups; for the first, RNA was extracted using exoquick treated serum, and in the second, RNA was extracted from total serum. Next, miRNA expression was analyzed using Agilent miRNA microarray. The above procedure was performed independently twice (**Fig. 1A**). We compared the miRNA expression pattern among the four microarray results (**Fig. 1B**) and found that miRNA expression analysis using exoquick was the more reliable and reproducible (**Fig. 1C**).

Exosome from normal human prostatic cell lines PNT-2, was yielded by the conventional ultra-centrifugation method [8]. We prepared serums with and without exoquick treatment and performed immunoblot analysis with anti-CD63 (**Fig. 1D**). Bands of the expected relative sizes were detected in serum treated with exoquick. We designated RNA extracted using exoquick treated serum as exosome-rich fractionated RNA.

Unique Expression Pattern of miRNA in CHC

We attempted to diagnose CHC using the miRNA expression pattern found in the peripheral blood samples from 64 CHC and 24 NL. The expression of nine miRNAs (miR-1225-5p, miR-1275, miR-638, miR-762, miR-320c, miR-451, miR-1974, miR-1207-5p, and miR-1246) allowed us to categorize patients as CHC or NL with 96.59% accuracy (**Fig. 2, 3** Table 1 and Table S1). As shown in **Fig. 2C**, CHC and NL were well differentiated due to their distinct miRNA expression patterns. The expression pattern of 12 miRNAs led to the distinction of CHC, CHB, NASH, and NL with 87.50% accuracy (**Fig. 4, S1A,** and Table S1). The accuracy of determining whether samples were CHC or CHB, CHC or NASH, CHB or NASH was 98.35%, 97.37%, and 87.50%, respectively. The accuracy of judging whether samples were NL or CHB, NL or NASH, was 89.29% and 88.89%, respectively (**Fig. 3, S1B** and Table S1). Unlike CHC and NL, there were relatively fewer analyses done of CHB and NASH (due to a small sample size), therefore, we used *"in silico"* resampling to overcome any possible bias. With *"in silico"* we found that it was highly reproducible to determine with high accuracy whether samples were CHC, CHB, NASH, or NL, CHC or CHB, CHC or NASH, CHC or NL, CHB or NASH, CHB or NL, or finally NASH or NL (**Fig. S2 to S8** and Supporting Information).

In order to validate our above-mentioned classifications, we prepared a separate independent sample consisting of 31 CHC, 16 CHB, and 8 NASH. We established miRNA expression patterns using microarray for each of these chronic liver disease groups. We tried to discriminate among the classifications in the independent cohort using the semi-supervised learning method [24] based only on the labels in the original sample group and the selected miRNAs shown in Table S1. The accuracy of judging whether samples were CHB or CHC, CHC or NASH, CHB or NASH, was 74.47%, 87.18%, and 79.19%, respectively (**Fig. S9**, Table 1, and Supporting Information). During the process of obtaining these results, we noticed that different versions of the Feature Extraction (FE) Software provided slightly different results, however it was not possible to fully unify these versions of FE. This may explain the relatively lower performance of the independent group compared with the original samples that mostly used the same FE Software versions.

miRNA Expression Correlates with the Grade of Liver Inflammation

The grade of inflammation for CHC patients was ascertained by liver histological examination, and then samples were divided into four groups A0, A1, A2, and A3 based on their fibrosis stage. miRNA expression profiles were then established for CHC according to each of their inflammation grade. From the four groups (A0 to A3), a combination of six arbitrary pairs is possible. miRNAs which had significant differential expression in five or more of the six pairs were extracted ($p<0.05$). Five miRNAs (miR-1914*, miR-193a-5p, miR-22, miR-659, and miR-711) had expression levels that increased as the severity of liver inflammation progressed. On the other hand, the expression levels of nine miRNAs (miR-1274b, miR-197, miR-1974, miR-21, miR-34a, miR-451, miR-548d-5p, miR-760, and miR-767-3p) significantly decreased with the progression of liver inflammation (**Fig. 5, S10** and Table S2).

The Grade of Liver Fibrosis Corresponded with the Expression Level of miRNAs

As previously noted, CHC samples were divided into F0, F1, F2, and F3 based on patients' fibrotic stage. From these four fibrotic groups, a combination of six arbitrary pairs were possible. miRNAs that had significant differential expression in all six pairs were extracted ($p<0.05$). The expression levels of two miRNAs (miR-483-5p and miR-671-5p) significantly increased the higher the fibrotic stage and the expression level of 14 miRNAs (let-7a, miR-106b, miR-1274a, miR-130b, miR-140-3p, miR-151-3p, miR-181a, miR-19b, miR-21, miR-24, miR-375, miR-548l, miR-93, and miR-941) became progres-

A

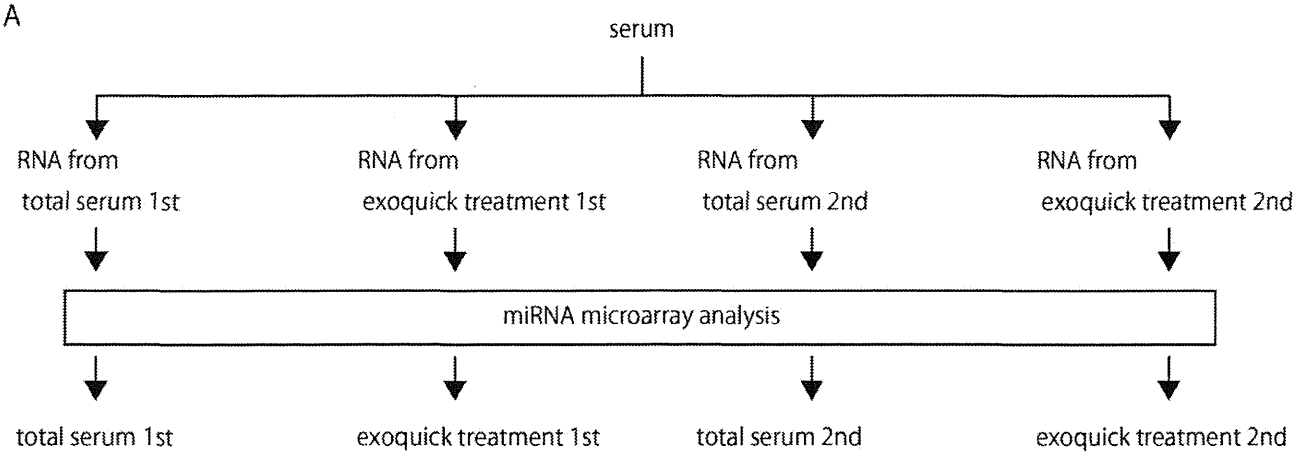

B

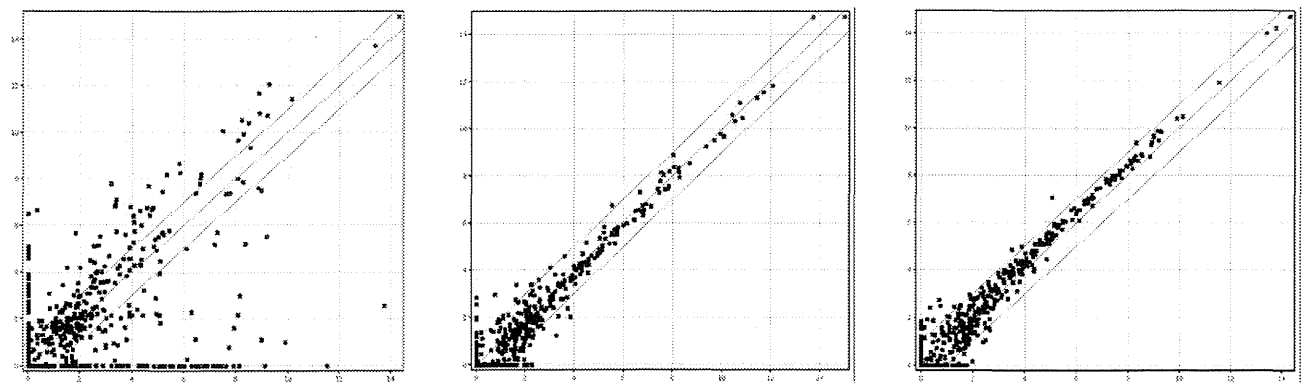

C

	exoquick 1st	total serum 1st	exoquick 2nd	total serum 2nd
exoquick 1st	1	0.836	0.998	0.809
total serum 1st	–	1	0.831	0.930
exoquick 2nd	–	–	1	0.821
total serum 2nd	–	–	–	1

D

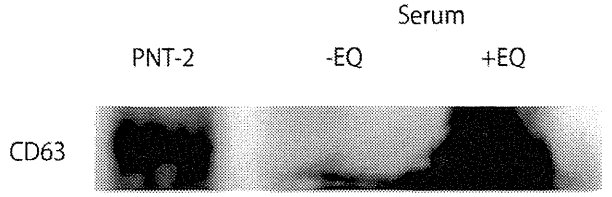

Figure 1. The method used to obtain reproducible data for microarray analysis conducted on serum-extracted samples. A. NL patients' serum were sampled twice. In the first, RNA was extracted first from untreated serum, and then extracted again from serum treated with exoquick. In the second serum sample, RNA was also extracted from both untreated serum and serum treated with exoquick. Microarray analysis was conducted for RNA in a total of four samples. B. Reproducibility test of microarray data. Scatter plots comparing non- normalized signal intensities of miRNAs in two independent experiments from human total serum and exosome rich fraction. Red and black denotes high and low miRNA expressions respectively. Total serum extracted first, versus exosome rich fraction first (left), total serum extracted first versus second (middle), and exosome rich fraction extracted first versus second (right). C. Pearson's pairwise correlations of signal intensities of miRNAs from human total serum and exosome rich fraction. D. Western blot was performed for untreated serum, serum extracted by exoquick and exosome fraction from PNT-2, using anti-CD63.

doi:10.1371/journal.pone.0048366.g001

A

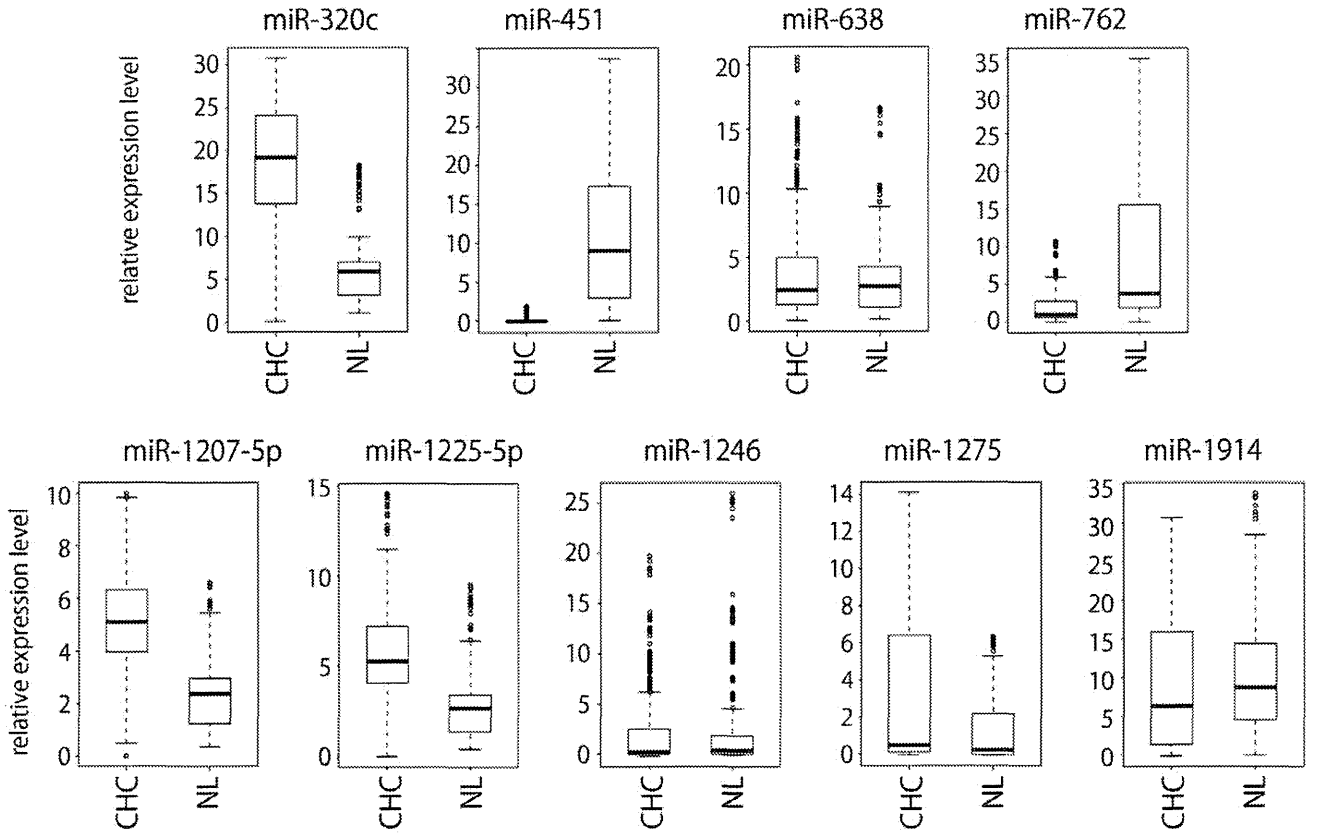

B

		result	
		CHC	NL
prediction	CHC	64	3
	NL	0	21

accuracy 96.6%

C

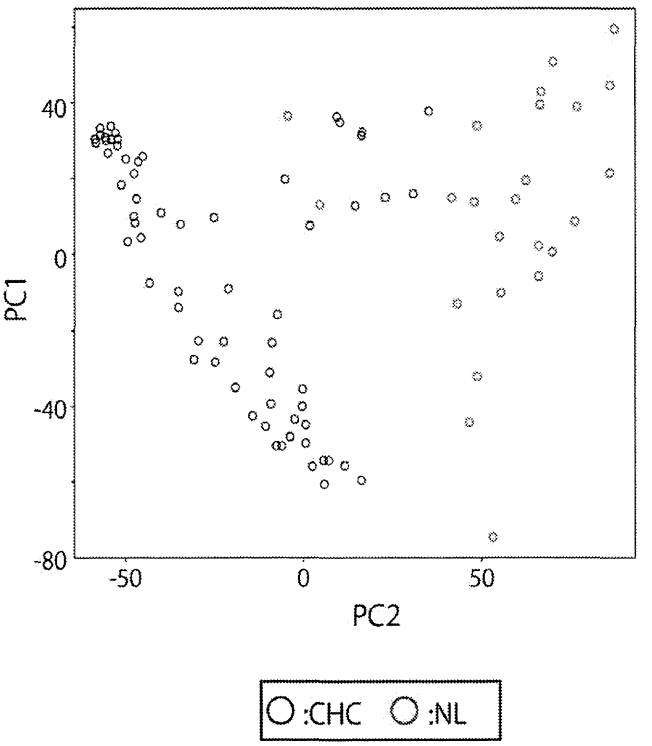

Figure 2. Expression patterns of miRNA used for discriminating between CHC and NL. A. Box plots of expression patterns of the nine miRNAs used for discriminating between CHC and NL. B. Classification of CHC and NL using LOOCV from miRNA expression profile. C. PCA in CHC and NL. The two dimensional embedding of CHC and NL by PCA. The first and second principal component scores computed (not selected for discrimination) of normalized miRNA expression were employed for this plot. Computation was done with ALL.
doi:10.1371/journal.pone.0048366.g002

sively downregulated as liver fibrotic stage increased (**Fig. 6, S11** and Table S2).

Classification of Liver Inflammation Grade and Fibrotic Stage Using miRNA Expression Pattern

We attempted to classify liver inflammation grade and fibrosis stage using miRNA expression pattern. Liver inflammation was diagnosed by Leave One Out Cross-Validation (LOOCV); the accuracy of determining A1 from other inflammation grade was 71.88% and its odds ratio was 7.08. The accuracy of determining A2 and A3 was 75.00% and 82.81%, and their odds ratios were 9.50 and 11.08, respectively. In our study, we were unable to accurately classify A0 because we were limited to only one sample for that grade (**Fig. 7A**). Diagnosis of liver fibrosis by LOOCV showed that determining F0 from the other fibrotic stages had an accuracy of 87.50% and an odds ratio of 14.25. The classification of F1, F2, and F3 had accuracy rates of 65.63%, 70.31%, and 73.44% and odds ratio of 3.16, 6.39 and 5.80, respectively (**Fig. 7B**).

miRNA Expression Level Detected by Real-time qPCR Validated the Microarray Result

Four miRNAs (miR-1207-5p, miR-134, miR-1249, and miR-1183) with expression levels that differed among liver inflammation grades and liver fibrotic stages were chosen in order to confirm the microarray results using stem-loop based real-time qPCR. miRNAs that correlated with other clinical characteristics besides liver fibrosis and inflammation were listed using the Wilcoxon test. We performed two Wilcoxon tests and ranked miRNAs based on their p-value from smallest to largest and selected the miRNAs with the four smallest p-values that were common among the two Wilcoxon tests.

The real-time qPCR result was consistent with the microarray analysis (**Fig. 8**). Here also, we applied *"in silico"* resampling to compensate for the small number of patients used in the real-time qPCR analysis. The results of the *"in silico"* resampling conferred with the results of the real-time qPCR (**Fig. S12**).

miRNA Expression Pattern was Closely Related to Several Clinical Parameters in CHC

Although we observed that miRNA expression correlated with ALT value, we were unable to identify miRNAs that displayed a strong correlation. 12 miRNAs were chosen sequentially from miRNAs with a high absolute correlation coefficient. One to 12 of these selected miRNAs were used to compare the canonical correlation coefficient of the above. When the expression patterns of six of the 12 miRNAs were compared with serum ALT value, the correlation coefficient and p-value were 0.44 and 4.91E−02, respectively. Similarly, when serum Albumin value was compared with the expression pattern of all 12 miRNAs, the correlation coefficient and p-value were 0.59 and 2.04E−02, respectively. Finally when the amount of serum HCVRNA was compared with the expression pattern of 12 miRNAs, the resulting correlation coefficient and p-value were 0.59 and 1.89E−02, respectively (**Fig. 9, S13** and Table S3).

Expression Pattern of a Several miRNAs Correlated to Serum and Hepatic Tissue

In a previous report, we described the miRNA expression pattern found in liver tissues obtained from 105 CHC [2]. From this group, we analyzed the miRNA expression of hepatic tissue and serum in 60 samples. We observed that the expression pattern of three miRNAs (miR-134, miR-200b, miR-324-5p) in hepatic tissue negatively correlated with that in serum, and the expression pattern of miR-370 in hepatic tissue positively correlated with that in serum ($p<0.05$) (Table S4). However, there was no significant correlation between the expression pattern of miR-122 in the hepatic tissue and serum (**Fig. S14** and Table S4).

Discussion

In this comprehensive miRNA analysis in various chronic liver diseases, we observed that aberrant expression of miRNAs was closely related to disease progression. Based on this, we believe that these miRNAs are potential readily accessible biomarkers, useful for diagnosing hepatic viral infection and for grading or staging liver diseases.

Many investigators have elected to use miRNA from serum instead of miRNA from exosome as the candidate for diagnosing diseases [18,20,22,25,26]. In our study, when exoquick was used, exosome could not be isolated therefore other MVs similar in size to exosome were also extracted. In other words, exoquick not only collected miRNAs contained in exosome, but also miRNA that were or were not combined with protein. Despite this, we found that exoquick delivered results that were superior to those obtained without exoquick. Therefore, although the process of analyzing miRNA from serum is simple, we chose to analyze miRNA from exosome rich fraction since it has a higher rate of reproducibility. Moreover, since exosome is closely related to intercellular signaling [14,27], it is expected that data obtained by exosome analysis can clarify the mechanism of chronic infection and inflammation [28].

When we extended our analysis from miR-122 to all miRNAs, it became clear that the expression level of several miRNAs correlated with the progression of liver fibrosis. In fact, recent studies have stated that when the expression levels of adequate numbers of miRNAs is used to identify disease, diagnostic ability is significantly higher than using a single miRNA [29]. In this study, when liver fibrosis was diagnosed using miRNA expression, distinguishing between F0 and F1-3 was done with 87.50% accuracy. Since F0 cannot be distinguished from other stages of chronic liver disease using blood examination, we propose that using miRNA expression pattern may be useful for diagnosing chronic liver disease that is in the early stage.

Previous studies have shown that the level of miR-122 in blood plasma increased earlier than in ALT in the presence of toxic liver injury in rodents [30]. Serum levels of miR-122 in patients with CHC are frequently elevated compared with healthy individuals [21]. Bihrer et al. mentioned that variations in the concentration of miR-122 in serum or plasma tend to be more specific for liver diseases than ALT and AST. This is because miR-122 is almost exclusively expressed in the liver, whereas ALT and AST originate from skeletal muscles and other tissues, therefore their diagnostic value is low [31]. In our study, the expression level of miR-122 had

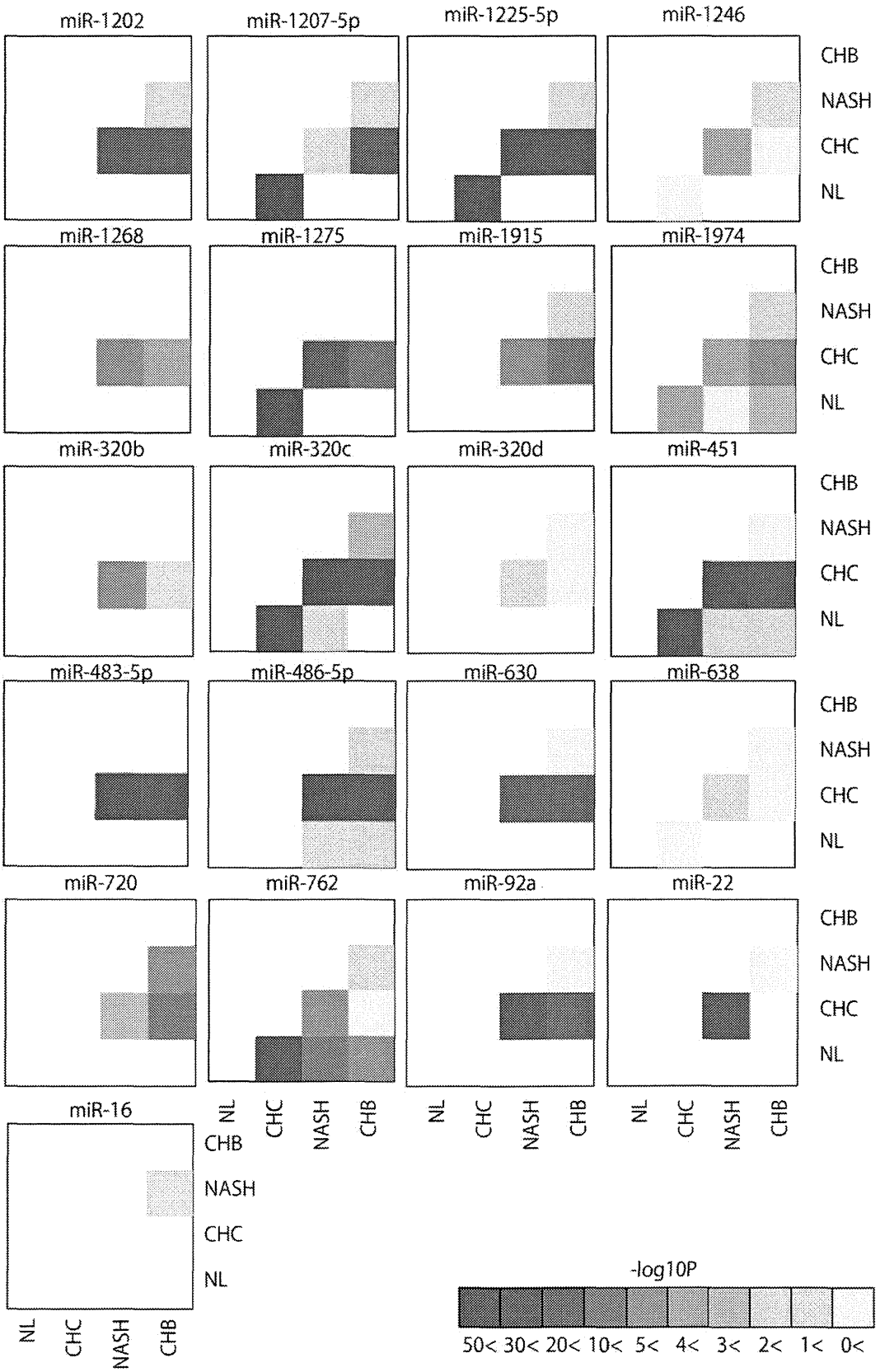

Figure 3. Pairwise heatmap of the miRNAs used for classifying two arbitrary groups. Pairwise heatmap showed the miRNAs and their p-value of two arbitrary groups.
doi:10.1371/journal.pone.0048366.g003

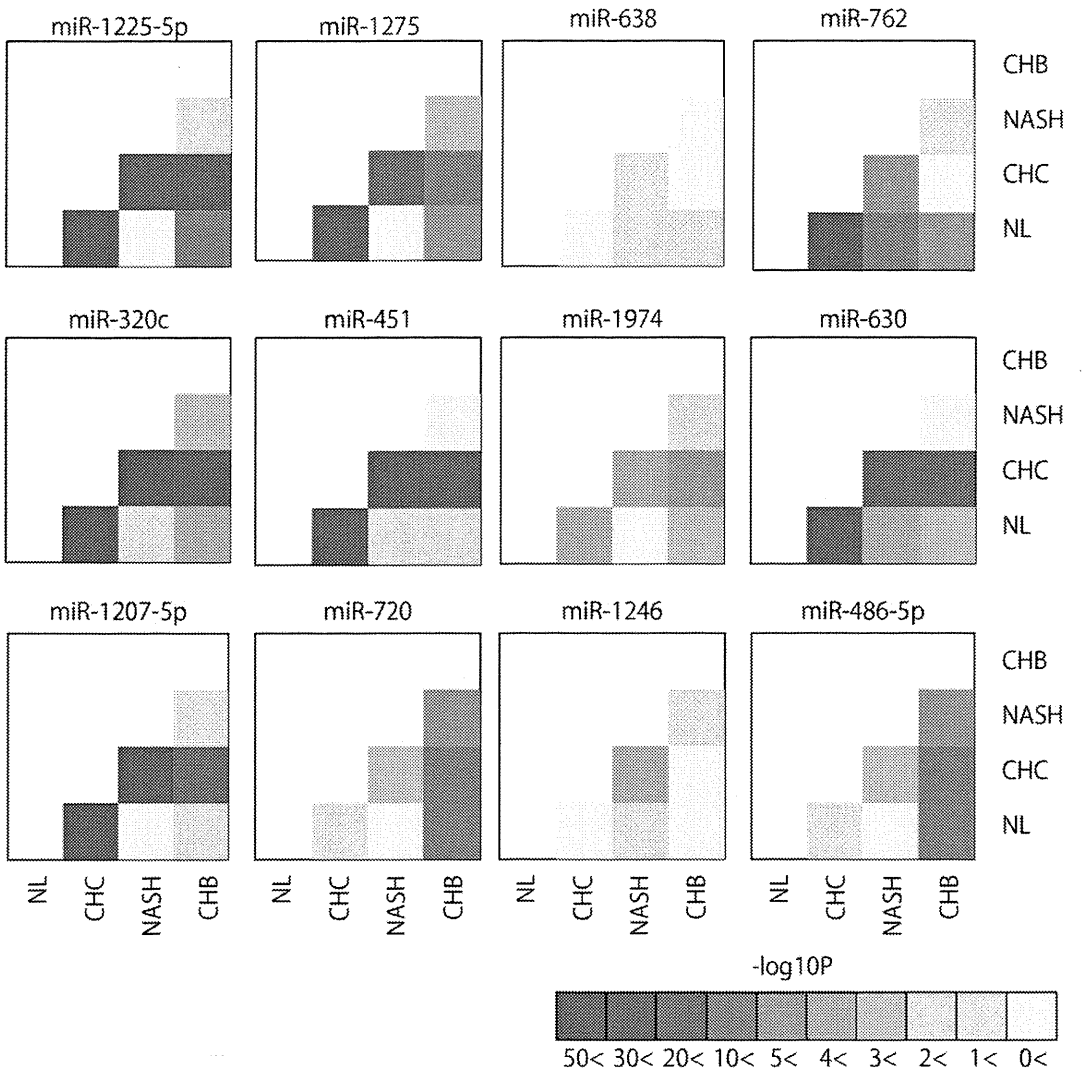

Figure 4. Pairwise heatmap of the miRNAs used for classifying among four groups.
doi:10.1371/journal.pone.0048366.g004

a significant positive correlation with the grade of liver inflammation, serum albumin value, or serum HCVRNA value. However, miR-122 expression did not significantly correlate with liver fibrosis stage. Moreover, there was no correlation between the expression level of miR-122 in liver tissue, and that in serum in the same 60 samples (**Fig. S14**). The expression pattern of only four miRNAs out of total liver tissue miRNAs correlated with the expression patterns of miRNA found in the serum (Table S4). Most serum miRNA had expression patterns that differed from those observed in hepatic tissue samples. Moreover, we observed differences in miRNAs expression between various tissues [32]. These differences were observed even in tissues taken from the same subject; at present we are unclear as to the reason for this phenomenon.

In regards to the progression of liver fibrosis and the expression pattern of miR-21, previous studies concur with our result that miR-21 expression level significantly decreased in response to the progression of liver fibrosis [20]. Taken together, this suggests that any miRNAs that may have been emitted from liver tissue cannot be detected in serum after hepatic cell injury.

The expression pattern of many miRNAs in serum positively correlated with serum ALT, albumin, and HCVRNA levels in this study (**Fig. 9, S13** and Table S3). This result contradicts prior assumptions that no correlation exists between serum miR-122 and HCVRNA serum levels [21]. Three likely reasons for this difference in results are: 1) the detection method used (real-time qPCR versus microarray), 2) the difference in the subjects' ages (the subjects in this study were older), and 3) the difference in the amount of miRNAs (multiple miRNAs vs. a single miRNA) used to identify the clinical parameters of the disease.

CHC and NL were classified with a high level of accuracy using the expression pattern of miRNA. In order to elucidate if the miRNA expression in CHC is common to other chronic liver diseases including CHB, we compared the miRNA expression pattern of CHC with those of NASH and CHB. The result of this analysis was that CHC could be clearly distinguished from both CHB and NASH. These results demonstrate that the varying forms of chronic liver disease have their own unique miRNA expression pattern. NASH is a histological diagnosis that rests on a combination of features and can only be confirmed by liver biopsy. Recently, NASH was diagnosed by first determining the existence of NAFLD from blood samples and then performing an ultrasound tomography. Finally, liver fibrosis stage was determined by Fibroscan

Table 1. Characteristics of subjects in this study of original samples and independent samples.

Original samples

Characteristics	CHC	CHB	NASH	NL
Gender	F: 34/M: 30	F: 2/M: 2	F: 3/M: 9	F:11/M: 13
Age (years)	59.5±8.3	46.8±14.5	52.3±13.1	50.8±12.0
AST (IU/L)	50.1±29.8	83.3±53.7	46.2±16.0	N.D
ALT (IU/L)	57.6±40.6	167.8±170.3	74.5±34.9	N.D
WBC (x10^3/mm^3)	5.1±1.5	4.7±1.5	6.2±1.6	N.D
Platelet (x10^4/mm^3)	16.6±5.9	14.8±6.3	24.7±8.0	N.D
Total Bilirubin (mg/dl)	0.65±0.22	0.83±0.40	0.76±0.25	N.D
Weight (kg)	57.9±9.18	58.8±4.3	74.9±24.8	59.6±9.6
ALP (IU/L)	267.0±88.4	223.3±25.0	232.7±36.2	N.D
γGTP (IU/L)	46.9±42.3	77.3±82.2	58.4±20.9	N.D
Hemoglobin (g/dl)	13.8±1.2	14.5±0.59	14.7±1.6	N.D
Albumin (g/dl)	4.1±0.4	4.2±0.5	4.4±0.3	N.D

Independent samples

Characteristics	CHC	CHB	NASH
Gender	F: 18/M: 13	F: 10/M: 6	F: 6/M: 2
Age (years)	59.5±8.3	46.8±14.5	54.8±12.7
AST (IU/L)	50.1±29.8	83.3±53.7	80.9±50.0
ALT (IU/L)	57.6±40.6	167.8±170.3	108.9±76.2
WBC (x10^3/mm^3)	5.1±1.5	4.7±1.5	5.5±1.8
Platelet (x10^4/mm^3)	16.6±5.9	14.8±6.3	19.3±7.6
Total Bilirubin (mg/dl)	0.65±0.22	0.83±0.40	0.73±0.25
Weight (kg)	57.9±9.18	58.8±4.3	66.4±9.9
ALP (IU/L)	267.0±88.4	223.3±25.0	278.6±100.6
γGTP (IU/L)	46.9±42.3	77.3±82.2	130.1±81.23
Hemoglobin (g/dl)	13.8±1.2	14.5±0.59	13.6±1.4
Albumin (g/dl)	4.1±0.4	4.2±0.5	3.8±0.3

Abbreviations; CHC, chronic hepatitis C; CHB, chronic hepatitis B; NASH, non alcoholic steatohepatitis; NL, normal liver (healthy control); N.D, no data.
doi:10.1371/journal.pone.0048366.t001

(reviewed in [33]). However, when the results of these and other measures fail to yield a diagnosis then a pathology evaluation is necessary. Using "*in silico*" resampling to increase the reliability of our data, has led us to believe that NASH diagnosis may be possibly through blood examination.

We tested the reliability of our analysis in two ways and obtained reproducible results in both cases. First we enrolled an independent sample group, and second, we created virtual cohorts using in silico resampling to overcome our small sample size.

In this study we concluded that miRNA profiling is a promising alternative to diagnosing liver disease. This is based on our demonstration that the following evaluations could be performed using suitable miRNA expression profiles (1) determining the stage or grade of chronic liver disease, (2) ascertaining the clinical status of chronic liver diseases, and (3) distinguishing among various forms of chronic liver diseases. While these results suggest there is great potential and benefit of miRNA profiling, future studies in a larger population of CHC patients are warranted to fully elucidate the diagnostic potential of serum miRNA expression.

Materials and Methods

Patient Selection

A cohort of 64 CHC, 4 CHB, and 12 NASH patients who had undergone liver biopsy, as well as 24 healthy control subjects was enrolled. We also prepared independent samples consisting of 31 CHC, 12 CHB, and 8 NASH to validate our results. Patient characteristics are summarized in Table 1 and detailed clinical data is depicted in Table S5. The criteria for exclusion for CHC, CHB, and NASH were: co-infection with human immunodeficiency virus (HIV) types 1 and 2, decompensated liver disease, organ transplantation, immune suppression, autoimmune disorders, consumption of >20 g/day alcohol, and past history of intravenous drug abuse. Healthy controls were selected if they were not infected with HBV, HCV, nor HIV, had normal liver function tests, and had no history of liver disease.

All patients or their guardians provided written informed consent, and Ogaki Municipal Hospital and Kyoto University Graduate School and Faculty of Medicine's Ethics Committee approved all aspects of this study in accordance with the Helsinki Declaration.

Liver Histology and Blood Examination

A liver biopsy specimen was collected from each patient before anti-viral treatment. Histological grading and staging of CHC liver biopsy specimens were performed according to the Metavir classification system [34]. NASH was diagnosed histologically [35].

Serum HCV RNA was quantified before IFN treatment using Amplicor-HCV Monitor Assay (Roche Molecular Diagnostics Co., Tokyo, Japan), while serum HBV DNA was quantified before treatment using Amplicor HBV Monitor Assay (Roche). Pretreatment blood tests were conducted to determine each patient's level of aspartate aminotransferase (AST), alanine aminotransferase (ALT), total bilirubin, alkaline phosphatase, gamma-glutamyl transpeptidase, white blood cell (WBC), platelets, and hemoglobin.

Blood Sampling

Peripheral blood was collected from all subjects directly into serum tubes before anti-viral treatment. The tubes were centrifuged at 1,500 *g* for 10 min at 4°C, sera were aliquoted and additionally centrifuged at 2,000 *g* to completely remove any remaining cells. Sera were stored at −80°C until use.

RNA Preparation

Total RNA from 200 ul of serum was prepared using miRNeasy mini kit (Qiagen, Hilden Germany) according to the manufacturer's instruction. Exosome rich fractionated RNA was prepared using Exoquick (System Biosciences, CA, USA). Briefly, 900 ul of serum was mixed with 250 ul of Exoquick and incubated for 12 hr at 4°C. The tubes were centrifuged at 1500 g for 30 min at room temperature and then supernatant was discarded. The pellet was dissolved with 200 ul of PBS with vigorous vortex. RNA was extracted using miRNeasy mini kit (Qiagen).

Immunoblot Analysis and Exosome Preparation

The procedure for exosome preparation has been previously described [8]. SDS-PAGE gels, SuperSep Ace 5–20% (194–15021) (Wako, Osaka, Japan), were calibrated with Precision Plus Protein Standards (161–0375) (Bio-Rad), and anti-CD63 (1:200)

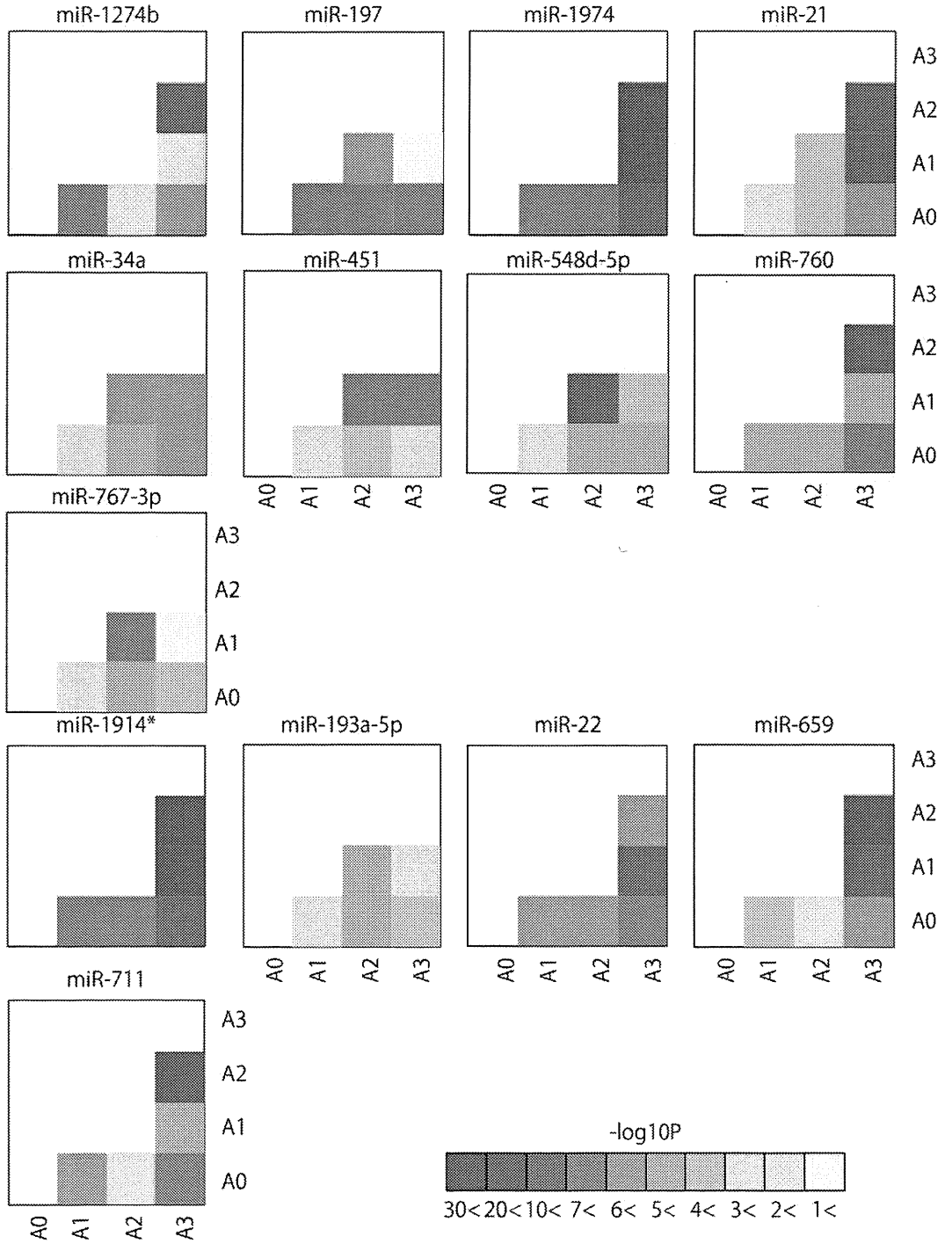

Figure 5. Significantly differentially expressed miRNAs according to liver inflammation grade. Pairwise heatmap showing the miRNAs and p-value of two arbitrary grades.
doi:10.1371/journal.pone.0048366.g005

was used as primary antibodies. The dilution ratio of each antibody is indicated in parentheses. Two secondary antibodies (peroxidase-labeled anti-mouse and anti-rabbit antibodies) were used at a dilution of 1:5000. Bound antibodies were visualized by chemiluminescence using the ImmunoStar LD (Wako) and luminescent images were analyzed by a LuminoImager (LAS-3000; Fuji Film, Inc.). Only gels for CD63 (BD, NJ, USA) detection were run under non-reducing conditions. To exclude the albumin and IgG in serum, Albumin & IgG Depletion SpinTrap kit was used (GE health care, WI, USA). After aliquots isolation, exosome-contained fraction was isolated by Exoquick according to standard instructions.

miRNA Microarray

To detect serum miRNA, 60 ng of RNA was labeled and hybridized using the Human microRNA Microarray Kit (Rel

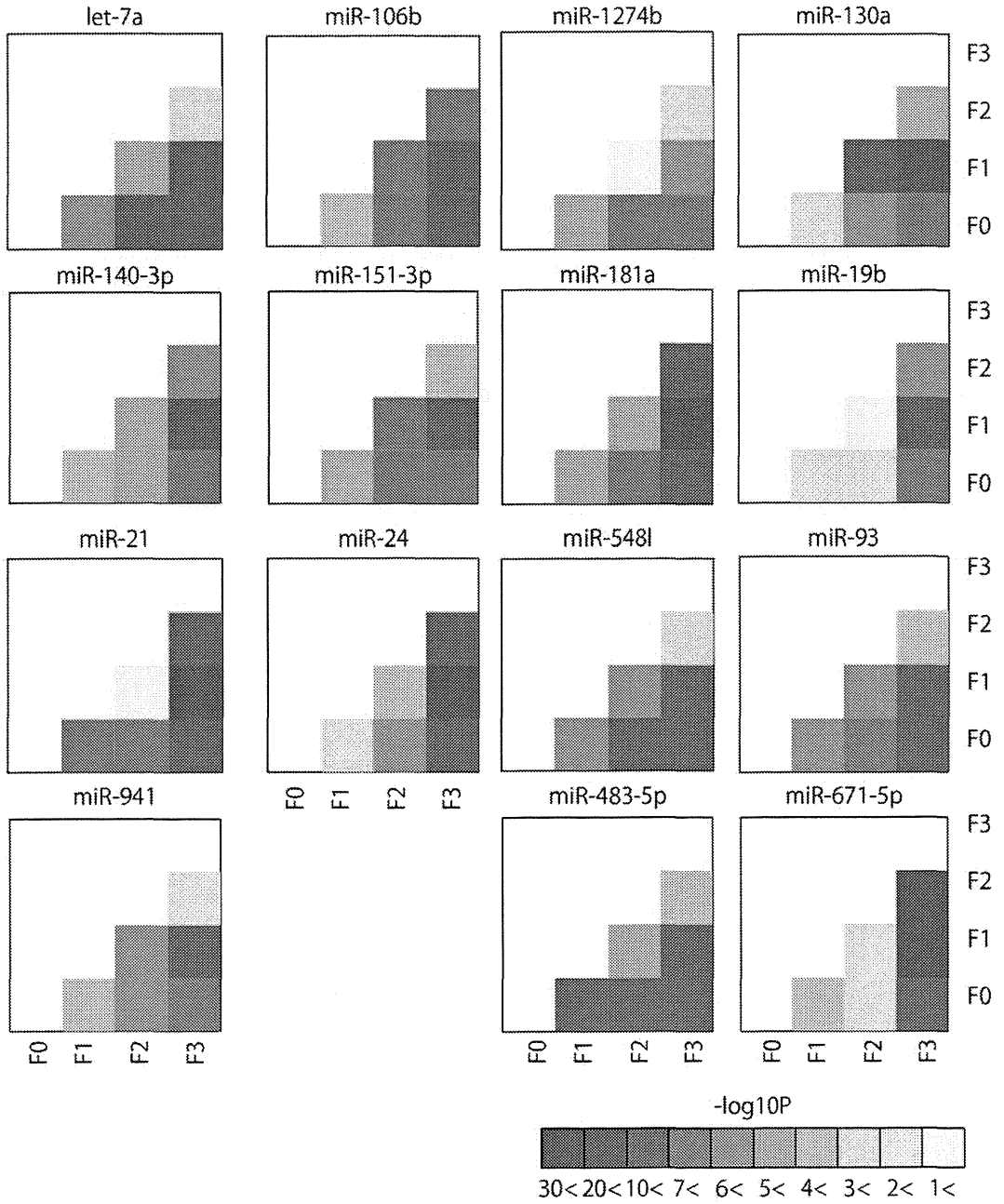

Figure 6. Significantly differentially expressed miRNA according to liver fibrotic stage. Pairwise heatmap showing the miRNAs and p-value of two arbitrary stages.
doi:10.1371/journal.pone.0048366.g006

14.0) (Agilent Technologies, CA, USA) according to the manufacturer's protocol (protocol for use with Agilent microRNA microarrays Version 1.0). Hybridization signals were detected with a DNA microarray scanner G2505B (Agilent Technologies) and the scanned images were analyzed using Agilent feature extraction software (v9.5.3.1). We used raw data (gProcessedSignal) and normalized each expression so as to have zero mean and unit sample variance. The data presented in this manuscript have been deposited in NCBI's Gene Expression Omnibus and are accessible through GEO Series access number GSE33857: http://www.ncbi.nlm.nih.gov/geo/query/acc.cgi?acc = GSE33857.

Real-time qPCR for Human miRNA

To detect miRNA expression level by real-time qPCR, TaqMan® microRNA assay (Applied Biosystems) was used to quantify the relative expression levels of miR-1207-5p (assay ID. 241060), miR-134 (assay ID. 000459), miR-1183 (assay ID. 002841), and miR-1249 (assay ID. 002868). The expression level of miR-16 (assay ID. 000391) was also measured and used as an internal control. cDNA was synthesized using the Taqman miRNA RT Kit (Applied Biosystems). RNA (2 ng/ml) in 5 ml of nuclease free water was added to 3 ml of 5 × RT primer, 10×1.5 μl of reverse transcriptase buffer, 0.15 μl of 100 mM dNTP, 0.19 μl of RNase inhibitor, 4.16 μl of nuclease free water, and 50 U of reverse transcriptase in a total volume of 15 μl. The reaction was performed for 30 min at 16°C, 30 min at 42°C, and 5 min at 85°C.